ELSEVIER

Biochimica et Biophysica Acta 1509 (2000) 14–41

BIOCHIMICA ET BIOPHYSICA ACTA
BBA

www.elsevier.com/locate/bba

Review

Advances in the characterization of supported lipid films with the atomic force microscope

Yves F. Dufrêne [a,*], Gil U Lee [b]

[a] *Unité de chimie des interfaces, Université catholique de Louvain, Place Croix du Sud 2/18, 1348 Louvain-la-Neuve, Belgium*
[b] *School of Chemical Engineering, Purdue University, West Lafayette, IN 47907, USA*

Received 27 July 2000; received in revised form 28 September 2000; accepted 3 October 2000

Abstract

During the past decade, the atomic force microscope (AFM) has become a key technique in biochemistry and biophysics to characterize supported lipid films, as testified by the continuous growth in the number of papers published in the field. The unique capabilities of AFM are: (i) capacity to probe, in real time and in aqueous environment, the surface structure of lipid films; (ii) ability to directly measure physical properties at high spatial resolution; (iii) possibility to modify the film structure and biophysical processes in a controlled way. Such experiments, published up to June 2000, are the focus of the present review. First, we provide a general introduction on the preparation and characterization of supported lipid films as well as on the principles of AFM. The section 'Structural properties' focuses on the various applications of AFM for characterizing the structure of supported lipid films: visualization of molecular structure, formation of structural defects, effect of external agents, formation of supported films, organization of phase-separated films (coexistence region, mixed films) and, finally, the use of supported lipid bilayers for anchoring biomolecules such as DNA, enzymes and crystalline protein arrays. The section 'Physical properties' introduces the principles of force measurements by AFM, interpretation of these measurements and their recent application to supported lipid films and related structures. Finally, we highlight the major achievements brought by the technique and some of the current limitations.

Keywords: Atomic force microscopy; Bilayer; Biomembrane; Lipid; Monolayer; Nanometer scale; Physical property; Structure; Surface force

1. Introduction

During the past decades, lipid monolayers and bilayers supported on solid substrata have attracted considerable interest, both from the fundamental and applied points of view. These model structures have been widely used to study the structure and properties of native biological membranes and to investigate biological processes such as molecular recognition, enzymatic catalysis, cell adhesion and membrane fusion [1–4]. On the other hand, a variety of applications relying on supported lipid films have been developed, including the design of biosensors [5,6], the biofunctionalization of inorganic solids [3], the crystallization of proteins [7–10] and the immobilization of DNA [11].

The Langmuir–Blodgett (LB) technique [12,13] is a well-established method to prepare supported monolayers and bilayers. By compressing a monolayer of

* Corresponding author. Fax: +32-10-47-20-05; E-mail: dufrene@cifa.ucl.ac.be

0005-2736/00/$ – see front matter
PII: S0005-2736(00)00346-1

lipid molecules spread on the air–water interface using a moving barrier, the phase of the lipid can be controlled. This monolayer may be transferred from the air–water interface onto solid substrates using either the LB [14] or Schaefer [15] transfer methods. Alternative methods for preparing supported lipid bilayers have been developed in recent years, including the design of bilayer membranes resting on ultrathin, soft polymer cushions [3] and the fusion of vesicles to hydrophilic supports [2,16–18], to supported lipid monolayers [19], or to alkanethiol-coated surfaces [20–23]. The later system, also called 'hybrid bilayer membrane' offers unique advantages over more conventional planar model membranes (for a recent review, see [24]): alkanethiols can form a complete hydrophobic layer at metal surfaces and provide the driving force for the formation of a complete bilayer; the strong association with the surface is insensitive to changes in buffer, pH, ionic strength or lipid composition; fabrication is easy since it only relies on self-assembly processes; due to their high mechanical stability, hybrid membranes can be kept intact and studied for months; finally, the use of a metal support allows the use of techniques that could not be applied otherwise, such as electrochemical techniques and surface plasmon resonance (SPR).

A number of techniques are available to characterize the structure, composition and properties of lipid films. The molecular organization and domain morphology in lipid monolayers at the air–water interface have been studied by fluorescence microscopy [25–27] and Brewster angle microscopy [28–30]. Insight into the fine structure and molecular order of lipid films has been gained by using X-ray reflection [31,32] and diffraction [26] methods and neutron reflectivity [22,33,34]. The lateral diffusion and lateral organization in lipid layers have been investigated with the fluorescence recovery after photobleaching technique [15,35–38].

Transferring lipid films onto solid substrata offers the possibility of applying a range of surface analytical techniques that could not be used to study real biological membranes. SPR, quartz crystal microbalance (QCM), surface enhanced Raman spectroscopy and reflection-absorption infrared spectroscopy allow monitoring of the formation of lipid films and the binding of biomolecules [6,21,22,24,39]. Ellipsometry is a convenient method for measuring the thickness of lipid films [22,40]. X-ray photoelectron spectrometry (XPS) can provide information not only on the chemical composition of supported lipid films but also on their molecular organization [41–44]. Time-of-flight secondary ion mass spectrometry (TOF-SIMS) allows detailed chemical analysis of lipid systems and visualization of micrometric domains [42,45].

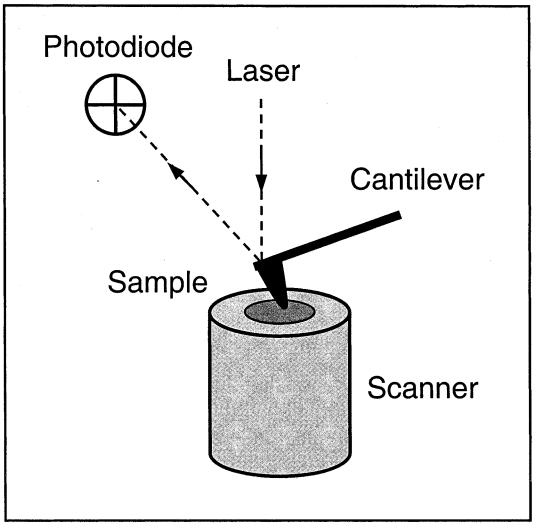

Fig. 1. Principle of AFM.

Despite this great variety of methods, little was known until recently about the structure and properties of lipid films at the nanometer level, due to a lack of high resolution surface imaging technique. The emergence of atomic force microscopy (AFM) ([46]; Fig. 1) has opened up exciting new possibilities in supported lipid film research. The unique advantages of AFM over other techniques can be summarized as follows: capacity to study, in real time and in aqueous environment, the surface nanostructure of lipid films and the conformational changes of individual molecules; ability to directly measure physical properties at high spatial resolution; possibility to perturb film structure and biophysical processes in a controlled way. These capabilities justify the continuous growth of AFM applications in lipid film research, as is evident from the continuous increase in the number of publications in this field (e.g. while only 10 papers were published in 1994, there has been more than 50 publications during the last year).

Different AFM imaging modes have been developed (for detailed information on the principles and different imaging modes of AFM, see [47–52]). In contact mode, sample topography can be measured in two ways, i.e. the 'constant-deflection' mode in which feedback is used to maintain a constant cantilever deflection and the 'constant-height' mode in which the cantilever deflection is recorded while the probe is scanned over the substrate with the feedback control loop disengaged. In tapping mode AFM (TMAFM) or intermittent contact mode, the probe is excited externally and the amplitude and phase of the cantilever are monitored near the resonance frequency of the cantilever. As sample and probe come into contact, a force is applied to the probe that results in a shift in the resonance frequency of the cantilever and in the amplitude of vibration at any frequency near resonance. This produces a sensitive feedback scheme and is well-suited for imaging soft materials since probe–sample lateral forces are greatly reduced.

In contact mode, lateral forces (friction) produce a torque on the cantilever, which can be detected by measuring the differential signal from the horizontal segments of the photodetector. Lateral force microscopy (LFM), which measures variations of probe–sample friction while imaging surface topography [53], is a valuable tool for revealing chemical heterogeneities at the sample surface [54–56].

Force–distance curves allow one to measure local physical properties and interaction forces. Two-dimensional force mapping can be performed by recording multiple force–distance curve arrays in the (x, y) plane. Force measurements provide direct insight into physical properties such as surface forces [57–59], binding forces between complementary biomolecules [60], stretching of individual molecules [61,62] and sample mechanical properties [63].

Finally, a few imaging modes introduced more recently enable us to probe the nanomechanical properties of biological samples. Force modulation measures the amplitude and phase shift of the cantilever while the sample or the probe is vibrated, thereby allowing spatial variations of viscoelasticity to be probed [64]. Phase imaging, a variant of TMAFM, is based on detecting the phase lag of the cantilever oscillation relative to the signal sent to the piezo driver of the cantilever. This mode offers exciting possibilities for the elucidation of variations in material properties such as adhesion, friction and viscoelasticity [65,66].

While the application of AFM in biological sciences has been the subject of several extensive reviews (see for instance [67–69]), reviews dealing specifically with the characterization of the structure and physical properties of supported lipid films were lacking. These measurements, published up to June 2000, are the focus of the present review.

2. Structural properties

This section focuses on the different applications of AFM for characterizing the structure of supported lipid films. We first describe studies dealing with homogeneous systems, i.e. films made of single components and which do not form a phase-separation: visualization of the molecular structure, both for lipid bilayers under water and mono-/multilayers in air (Section 2.1.1); formation of structural defects (Section 2.1.2); effect of external agents (solvents, ions, enzymes and antibiotics) on the film structure (Section 2.1.3) and formation of supported films (Section 2.1.4).

We then focus on the organization (domain shape, molecular orientation) of phase-separated films: single component films prepared in the coexistence region (Section 2.2.1); films composed of mixtures of different lipids (Section 2.2.2) and of mixtures of lipids with other biomolecules such as glycolipids, lipopeptides and proteins (Section 2.2.3).

Finally, the use of supported lipid bilayers as a support for anchoring biomolecules, i.e. individual molecules (DNA, enzymes) (Section 2.3.1) and crystalline protein arrays (Section 2.3.2), is reviewed.

2.1. Homogeneous lipid films

2.1.1. Molecular structure

For the first time, the high resolution of AFM has enabled direct visualization of the lipid headgroups of supported lipid bilayers in aqueous solution. High resolution images of dimyristoylphosphatidylethanolamine (DMPE) and dimyristoylphosphatidylglycerol (DMPG) phospholipid monolayers on octadecyltrichlorosilane-coated mica were obtained in buffer so-

lution [70,71]. Parallel ridges of 0.9 nm in spacing and unit cells occupying 0.5 nm^2 were visualized for DMPE and DMPG, respectively, and attributed to lipid headgroups. These molecular arrangements, substantially different from that of mica, agreed with 3D crystal data available for the molecules. Zasadzinski et al. [72] imaged, under water, DMPE LB bilayers deposited on mica. The dominant features of the images were long, uniformly spaced rows about 0.8 nm in spacing and modulations along the rows with rounded bright spots every 0.5 nm. It was possible to push through the bilayer to image the mica lattice underneath by increasing the applied force. The observed spots were therefore attributed to the individual headgroups of the DMPE molecules, in agreement with X-ray and electron diffraction measurements. AFM images of polymerized LB bilayers of diynoylphosphatidylcholine (DAPC) under water revealed rows of headgroups 1.1 nm apart from each other [73]. The surface of hydrated dipalmitoylphosphatidylethanolamine (DPPE) LB bilayers showed parallel ridges with a period of 0.5 nm corresponding to rows of aligned headgroups consistent with known crystallographic structure [74].

The molecular structure of various supported lipid mono/multi-layers in air has also been resolved. Molecularly resolved images displaying the organization of hydrocarbon chains were reported for dimyristoylphosphatidylcholine (DMPC) [75] and DPPE [44] LB trilayers. In a study of the mode of assembly of the phospholipid cardiolipin on mica, Muscatello et al. [76] measured lattice parameters with a resolution of about 0.2 nm, in agreement with transmission electron diffraction data. AFM images of supported dipalmitoylphosphatidylcholine (DPPC) bilayers [77] and liposomes [78] in air showed molecularly resolved features with a periodicity close to that of the crystalline headgroups.

For LB monolayers, the surface pressure at which the films are transferred is a key factor influencing the film organization. Zhai and Kleijn [79] demonstrated that DPPC monolayers transferred at a pressure corresponding to the liquid-condensed (LC) phase showed a very regular and densely packed structure, individual methyl ends of the phospholipid chains being resolved; in contrast, monolayers obtained at a surface pressure corresponding to the LC/liquid-expanded (LE) coexistence phase showed less ordered regions while no regular structure was found in the LE phase.

Another important issue associated with molecular images of supported monolayers concerns the effect of the underlying substratum on the film organization. Chunbo et al. [80] found that the lattice structure of mica influenced the molecular arrangement of DMPC LB monolayers while increasing the number of deposited layers apparently eliminated this effect.

Besides lipid films, it is worth noting that a variety of fatty acid monolayers and multilayers have been imaged down to molecular resolution [81–85]; however, these studies are beyond the scope of this review.

2.1.2. Structural defects; lipid film stability

Several factors have been shown to induce the formation of defects in supported lipid layers and to affect their stability, desorption associated with the LB transfer being one of these. Using TMAFM in water, Bassereau and Pincet [86] visualized subnanometric holes in LB bilayers made of a first monolayer of DMPE and of an upper monolayer of dioleoylphosphatidylcholine (DOPC), which were attributed to the desorption of lipids of the first monolayer during the transfer of the second layer. The authors concluded that supported asymmetric bilayers are rarely homogeneous, i.e. bare mica may be exposed to the solution in very localized areas while some lipids from the inner layer may be present in the outer layer, a finding which may have major implications as regards interpretation of data obtained by techniques that lack lateral resolution, such as the surface forces apparatus.

The transfer pressure is another key factor that controls defect formation. For hydrated DPPC LB bilayers in the solid state, very few defects were found at 45 mN/m [87], while the defect coverage increased significantly at 25 mN/m. Branched (triple and quadruple chain) phospholipid monolayers transferred by the LB technique on various supports revealed pinholes on a submicrometer scale, the fraction of which could be reduced by increasing the film surface pressure [88].

The nature of the lipids can also play a role in determining the defect characteristics. Rinia et al. [89] found that the shape of the defects in asymmetric LB bilayers was influenced by the nature of the

first leaflet: polygonal line-shaped defects were observed with phosphatidylcholine (PC), whereas mainly round defects were seen with phosphatidylethanolamine (PE). In most of the PC-containing systems, the defects were surrounded by elevations referred to as bilayer blistering and attributed to phospholipid exchange between the two leaflets around the defects.

Fang and Yang [90] demonstrated the crucial influence of temperature on the lipid-loss process for supported DPPC bilayers prepared by vesicle fusion. The creation and growth of bilayer defects was observed as lipid molecules were lost from the bilayer. The rate of the lipid loss was very slow and had an Arrhenius behavior. At temperatures above 45°C, interdigitated membrane domains were induced and were mostly in contact with some bilayer defects.

Physical treatments such as the exposure to ultrasound or to the air–water interface have been shown to induce defect formation or film reorganization. The effect of ultrasound on DPPC lipid bilayer structure was investigated with the aim of a better understanding of the issues associated with transdermal drug delivery [91]. Bilayer defects, with average diameters of tens to hundreds of nanometers, were generated within less than 0.5 min as detected by AFM, the number of defects growing with time. The defect growth rate at the 168 kHz frequency was about 3.5 times that at the 707 kHz frequency. Vikholm et al. [92] reported holes of various sizes in DMPC layers in air obtained by spreading from vesicle suspensions onto supported arachidate multilayers. Transferring supported DPPE bilayers into the air was shown to reorganize the upper layer to form bilayer domains superimposed on top of the homogeneous lower layer [44].

The possibility to apply local forces in a controlled way with the AFM has been exploited to modify lipid films and to gain insight into their stability. Bilayers made of upper monolayers of distearoylphosphatidylcholine (DSPC) or DPPE were stable to continued rastering by the AFM probe; in contrast, upper layers of dilinoleoylphosphatidylethanolamine (DLPE) were much less stable, the stability depending on the pH of the aqueous environment [74]. The tangential stress exerted by the probe on the deformable DLPE monolayers eventually produced a ripple pattern, described as a periodic buckling known as Shallamach waves. Similar structures were observed for dipentadecanoyl-glycero-phosphatidylcholine bilayers [93]. Repeated scanning in contact mode shifted the random topology of the surface of PC bilayers to a striped pattern [93].

Damages were created with an AFM probe in DPPC and DPPE bilayers prepared either by detergent dialysis or by the adsorption of vesicles [94]. Hollow cylinders of diacetylenic phospholipid bilayers deposited on graphite were structurally modified using AFM [95]. The bilayer was imaged, cut or annealed based on the magnitude of the applied force. Cuts were repaired by scanning with a controlled force and driving lipids back into the cut; a slow self-annealing of cuts was also reported. The different layers of DPPC/DPPE trilayer systems in air were removed by varying the force applied by the probe [96].

Finally, different treatments have been shown to prevent defect formation or film reorganization, among which the incorporation of certain molecules or UV-irradiation. The addition of cholesterol was found to prevent hole formation and to generate surface bumps attributed to partially fused liposomes for membrane-mimetic lipid films prepared by fusion of lipid vesicles on alkylsilane-coated glass [97,98]. The stability of these systems was compromised when operating above the phase transition temperature of the lipids as well as in the presence of albumin. Viitala and Peltonen [99] found that optimum orientation and packing density of the DLPE molecules in monolayers were achieved by adding uranyl acetate to the subphase; however, the long-term stability of these films proved to be poor, clear reorganization and loss of a true monolayer structure being evidenced by the AFM images. This instability was inhibited for UV-irradiated films, indicating that the UV-irradiation gave rise to a cross-linked structure.

2.1.3. Effect of external agents

The effect of external agents such as solvents, ions, enzymes or antibiotics on the structure of supported lipid films is another area where significant breakthrough has been made owing to the advent of the AFM. Mou et al. [18] demonstrated that acyl chain interdigitation can be induced reversibly by alcohol

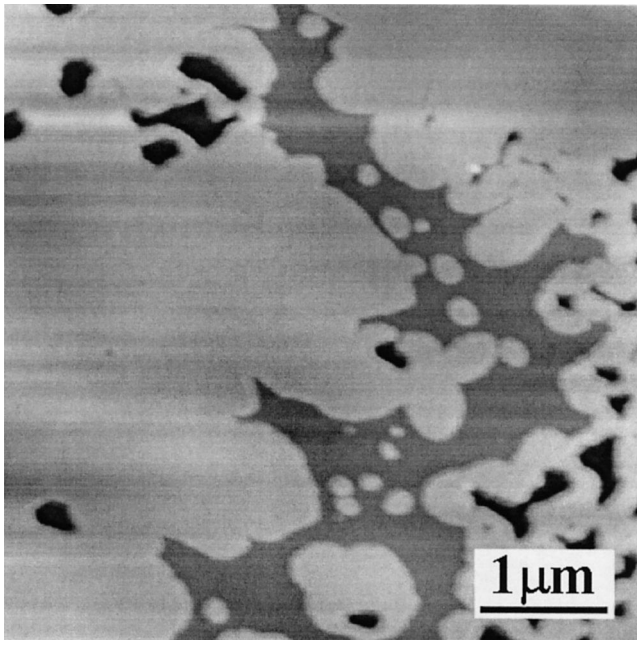

Fig. 2. AFM topographic image showing the induction of acyl chain interdigitation by ethanol (2.5% v/v) in supported DPPC bilayers (courtesy of Professor Z. Shao, University of Virginia, Charlottesville, VA, USA).

in supported DPPC bilayers (Fig. 2); interdigitation was demonstrated at alcohol concentrations far below previously described threshold values.

Under certain conditions, PC bilayers exhibit regular, large scale spatial modulation referred to as the ripple phase [78,100–102]. Using AFM, sodium and phosphate were shown to be necessary for the formation of the ripple structure in asymmetric bilayers composed of DPPC and 1-palmitoyl-2-oleoylphosphatidyglycerol (POPG), demonstrating a dependency for specific ions for this phase ([101]; Fig. 3). Along the same line, long-range ordered stripe domains were found in DPPC monolayers prepared on the subphase of lanthanide ion solutions [100].

The addition of Ca^{2+} to mixed bilayers made of negatively charged and neutral lipids induced phase-separation [69], in agreement with data obtained with other techniques. As detailed below (Section 2.2.2), the presence or absence of Ca^{2+} in the subphase was found to have a dramatic effect on the organization of phase-separated supported phospholipid bilayers containing mixtures of DPPC and dioleoyl phosphatidylserine (DOPS) or DOPC [103].

A better understanding of lipase enzyme activity on lipid film structure has been achieved. Turner et al. [104] explored the activity of free phospholipase C on a chemisorbed DMPC lipid film using a combination of AFM, XPS and SIMS. Nearly complete removal of the phosphate from the lipid layer was observed, indicating enzymatic activity of the phospholipase. Grandbois et al. [105] reported direct imaging of the degradation of supported DPPC bilayers by phospholipase A_2 with a lateral resolution of less than 10 nm. They demonstrated that the enzyme hydrolyzes the bilayer only in regions where defects are present and that it exhibits a preference for particular molecular orientations of the lipids. Well-defined channels with width comparable to the diameter of a single phospholipase were observed, supporting the idea that they result from the action of single enzymes. The kinetics of the phospholipase A_2 hydrolysis of bilayers may exhibit so-called 'lag-burst' behavior where the rate of hydrolysis suddenly changes from a low activity regime to a regime of rapid hydrolysis. Using in situ AFM, Nielsen et al. [106] showed growing nanoscale indentations in DPPC bilayers during the lag phase, attributed to domains of hydrolysis products; the

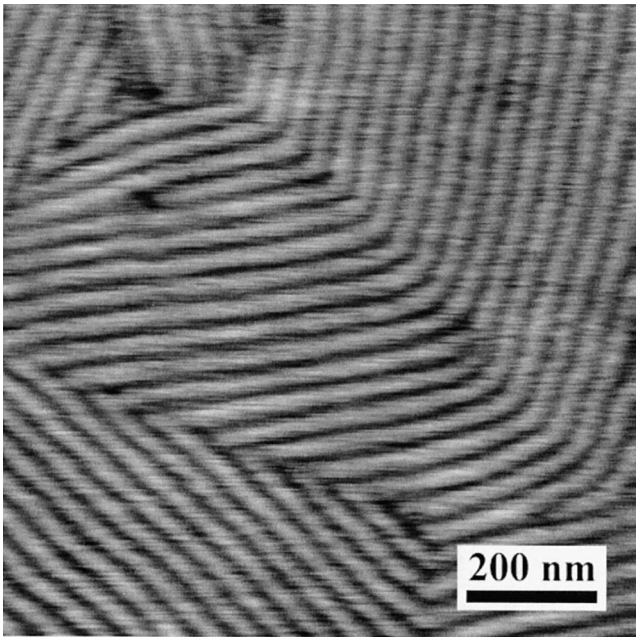

Fig. 3. Formation of the ripple structure in asymmetric bilayers of DPPC/POPG, as visualized by AFM at room temperature (courtesy of Professor Z. Shao, University of Virginia, Charlottesville, VA, USA).

rate of the rapid hydrolysis following the burst was found to be proportional to the length of the bilayer edge.

Various antibiotics were found to affect the structure of supported lipid films. The effect of filipin, an antibiotic with antifungal activity, on the integrity of DPPE bilayers was investigated, in the presence and absence of cholesterol [107]. Filipin-induced lesions were only found in membranes with cholesterol. In close agreement with electron microscopy results, circular and doughnut-shaped protrusions were detected in the membrane and attributed to filipin–cholesterol complexes. Through in situ AFM and QCM experiments, Ha et al. [108] obtained detailed information about the interaction of indolicidin, a tridecapeptide amide with antimicrobial activity, with dipalmitoylphosphatidic acid (DPPA) lipid membranes. The interaction occurred very rapidly with numerous holes (30–100 nm) being observed. With time, the disappearance of holes was noted and attributed to the incorporation of indolicidin molecules.

2.1.4. Formation of supported films

In recent years, the AFM has made it possible to monitor the formation of supported lipid films in situ, thus in a more direct way than using conventional surface analytical techniques such as infrared spectroscopy, X-ray or fluorescence microscopy. The dynamic topography change of PC and PE liposomes from a vesicle form to a flat bilayer through their direct adhesion on a mica surface was recorded by in situ AFM [109]. The liposomes adhered immediately on the mica surface and the spherical shape of the vesicles ruptured spontaneously and deformed to a flat supported film on the mica. In the PC liposome system, contrary to the PE system, the second bilayer was hardly formed. The formation rate of the PC bilayer depended on the salt and vesicle concentrations in the medium and increased with increasing content of these materials. On the other hand, in the PE liposome system, a vertical growth of lipid molecules was recognized. The different behaviors of PC and PE systems was interpreted by the existence of a hydration layer around the PC surface. Reviakine and Brisson [110] studied the early stages of growth of supported zwitterionic phospholipid bilayers by vesicle fusion on mica. Unilamellar vesicles of various sizes, prepared by sonication or extrusion, were found to adsorb to mica. Unruptured vesicles forming supported vesicular layers, as well as disks, formed as a result of vesicle rupture, could be visualized. The behavior of the supported vesicular layers was found to depend on the vesicle size, the lipid concentration and the presence or absence of Ca^{2+}. The effect of Ca^{2+} on the formation of phospholipid bilayers by vesicle fusion on mica was also studied by Kolb et al. [111]: in the absence of Ca^{2+}, vesicles adsorbed but did not fuse, while addition of Ca^{2+} induced the fusion process.

Tang et al. [112] investigated the formation of a model membrane bilayer structure consisting of a DMPC monolayer on an inner layer of a self-assembled monolayer (SAM) of octadecyltrichloroorganosilane (OTS) on mica. LFM and AFM images of OTS-coated mica immersed in DMPC solutions for varying exposure times showed that before forming a complete monolayer the molecules aggregated into dense islands (about 2.4 nm high) on the surface. The islands had a compact and rounded morphology. The rate constant of DMPC growth was calculated to be about 20 s^{-1} M^{-1}.

Carlson et al. [113] demonstrated that the AFM can be used to initiate bilayer fusion of high density lipoproteins (HDLs), which are responsible for the transport of cholesterol, in a controlled manner, allowing the fabrication of stabilized, nanometer scale, phospholipid bilayer domains. AFM imaging in fluid of DPPC/cholesterol liposomes decorated with small amounts of human IgG showed balloon-like structures with apparent diameters of 200–300 nm, in agreement with the mean size of liposomes deduced from previous dynamic light-scattering experiments [114].

With the aim of investigating the specific adhesion of unilamellar vesicles on functionalized surfaces mediated by molecular recognition, AFM and QCM were used to study adhesion of liposomes consisting of 1,2-dipalmitoyl-*sn*-glycero-3-phosphocholine and varying concentrations of *N*-((6-biotinoyl)-amino)hexanoyl)-1,2-dihexadecanoyl-*sn*-glycero-3-phosphoethanolamine (biotin-X-DHPE) [115]. With increasing biotin concentration, the height of the liposomes decreased considerably up to the point where vesicle rupture occurred. The firm attachment of the spread bilayers was proposed to explain un-

expected high frequency shifts of the quartz crystal (>500 Hz).

2.2. Phase-separated films

Membrane constituents, phospholipids, glycolipids and (glyco)proteins, are known to be organized in lateral domains in biomembranes [116–120]. This organization is thought to reflect the functional specialization of different regions of the membrane and to play an important role in membrane interaction processes. Hence, understanding the lateral interactions of lipids and proteins within mono- and bilayers is a key issue in membrane biophysics. In addition, heterogeneous lipid films can be used to design surfaces patterned with well-defined functionalities, which has a great potential in nanotechnology and biosensor technology. AFM has emerged as a key technique to investigate the lateral organization of phase-separated lipid films on the nanometer scale, i.e. beyond the resolution limit typically achieved at the air–water interface with fluorescence and Brewster-angle microscopy. This important topic is reviewed in the following paragraphs as follows: single component films prepared in the coexistence region (Section 2.2.1); films composed of mixtures of different lipids (Section 2.2.2) and of mixtures of lipids with other biomolecules such as glycolipids, lipopeptides and proteins (Section 2.2.3).

2.2.1. Pure lipid monolayers in the phase coexistence region

Several groups have observed the nanomorphology of single component lipid monolayers prepared in the region of coexisting phases. Yang et al. [121] showed that the domain structure in supported DPPC monolayers is influenced by the transfer pressure: at low pressure, small circular domains (50 nm in diameter) were observed while increasing the pressure caused an increase of domain size. In the LE/LC phase coexistence region, large (20 μm in diameter) domains with complex shapes were observed; high rates produced complex domain patterns with broken edges. The same team found that, in the phase coexistence region, DPPC monolayers can form two-dimensional chiral morphologies, most with two-, three-, four- or six-fold rotation symmetry; this was directly related to the enantiomorphic configuration of the lipids composing the monolayer coexistence region [122].

AFM topographic and friction images of thiolipid monolayers deposited on gold (chemisorption) and on mica (physisorption) in the region of coexisting phases revealed solid domains surrounded by a fluid phase [123]; differences in the structure and stability of the films were attributed to the different substrate/film interactions.

Masai et al. [124] used topographic and friction imaging for visualizing phase-separated structures attributed to the coexistence of LE and LC domains in single component PE, PC and synthetic lipids films adsorbed on carbon-coated silicon.

The influence of relative humidity (RH) on the structure of phase-separated DPPC monolayers in the region of coexisting phases was studied with TMAFM [125]. As the RH was increased above 65%, the small LE and LC domains became mobile on the surface and aggregated to form larger domains of like phase.

Exciting prospects for investigating lipid domain structures are now offered by near-field scanning optical microscopy (NSOM), a recent scanning probe microscopy combining the fluorescence contrast of conventional optics with the spatial resolution of a few tens of nanometers [5,126,127]. Horiuchi et al. [128] demonstrated that the topographic, friction, fluorescence and surface potential distributions of phase-separated fluorescently labelled phospholipid monolayers in the region of LE and LC coexisting phases can be simultaneously observed using a combined NSOM–AFM. Shiku and Dunn [129] presented high resolution NSOM fluorescence images of DPPC LB monolayers doped with a fluorescent dye showing distinct stripe patterns of coexisting phases. Fluorescence images of DPPC monolayers were also recorded at the air–sucrose solution interface using tapping mode force feedback [130].

2.2.2. Films made of lipid mixtures

AFM has shown to be a powerful tool for revealing nanoscale phase-separation in supported films made of lipid mixtures. A number of reports have focused on phase-separated supported monolayers in air. Phase-separation was revealed in LB monolayers made of mixtures of lipids found in the stratum corneum, i.e. ceramides, cholesterol and free

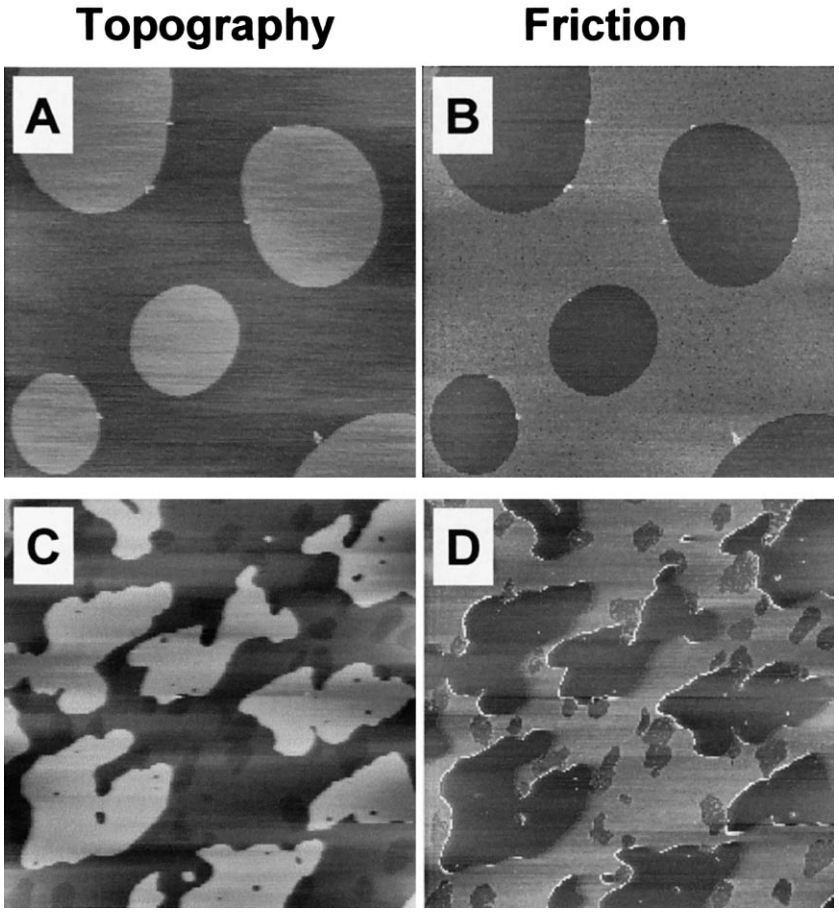

Fig. 4. Topographic (A, C) and friction (B, D) images (15×15 μm) of monolayers in air (A, B) and bilayers under water (C, D) made of a mixture of saturated DSPE and unsaturated DOPE.

fatty acids [131]. LB monolayers of DPPE and dioleoylphosphatidylethanolamine (DOPE) mixed in various proportions showed two coexisting phases due to immiscibility of the two lipids [132]. Lateral force images showed more friction on the liquid-like DOPE than on the solid-like DPPE, which was related to differences in lipid molecular packing. Both the molar fraction and the surface pressure played an important role in determining the shape and size of the domains.

Along the same line, AFM topographic and friction imaging of mixed monolayers made of distearoyl-phosphatidylethanolamine (DSPE) and DOPE showed phase-separation in the form of circular DSPE domains embedded in a DOPE matrix ([133]; Fig. 4). The step height measured between the higher DSPE phase and the lower DOPE phase (∼1.3 nm) was larger than expected due to a difference in the film mechanical properties. This was directly supported by the observation of inverted topographic and friction contrasts.

DeWolf et al. [134] investigated mixed monolayers of DSPC and phosphatidylinositol (PI), a component of lipid membranes which plays a major role in cellular functions. The films showed phase-separation as revealed by Brewster angle microscopy and AFM. DSPC formed a condensed monolayer with a centered rectangular structure and tilt towards nearest neighbors while PI formed a fluid monolayer with no lateral structure at all pressures investigated.

Phase-separation has also been demonstrated for various types of mixed lipid bilayer systems under water. In an early work, Weisenhorn et al. [135] recorded AFM images of hydrated bilayers made of a

mixed (19:1) upper layer of DMPE and biotinylated DPPE on DPPE-coated mica revealing the coexistence of fluid and crystalline domains.

Dufrêne et al. [133] observed phase-separation for mixed DSPE/DOPE bilayers under water. Compared to monolayers in air, the shape of the DSPE domains was more complex (Fig. 4). Furthermore, interpretation of the topographic contrast was difficult due to the influence of both mechanical properties and short-range repulsive surface forces (see Section 3).

The presence or absence of Ca^{2+} in the subphase was found to have a dramatic effect on the organization of phase-separated supported phospholipid bilayers containing mixtures of phospholipids in gel (DPPC) and fluid (DOPS or DOPC) states [103]. In the absence of Ca^{2+}, large, well-defined DPPC domains were found in both the DPPC/DOPC and DPPC/DOPS mixtures, while in its presence small, isolated DPPC domains were found in the DPPC/DOPS mixture. Ca^{2+} had no effect on the organization of DPPC in DPPC/DOPC mixtures, and its effect was abolished by adding DOPC to DPPC/DOPS mixtures.

AFM was used in combination with coherent scattering of evanescent neutrons to probe the geometry of domains in phospholipid bilayers of binary mixtures of synthetic lecithins (DMPC, DPPC, DSPC and DAPC) [136]. Grazing incidence diffraction of neutrons provided gel domain sizes of less than 10 nm in both the gel and the coexistence phase of the mixture, while no domains were detected for the fluid phase. The gel phase observed by AFM showed a rather irregular domain shape with an average size of 10 nm, thus confirming the neutron results.

Valdrè et al. [137] demonstrated the coexistence of nanoscopic domains in membranes prepared from liposomes made of a mixture of PLPC (1-palmitoyl-2-linoleoyl-3-phosphatidylcholine) and different amounts of cardiolipin (tetra-acyl-diphosphatidylglycerol). They also found that the process of controlled lipid peroxidation deletes the lateral phase-separations. These results were taken as experimental evidence for the hydrophobic mismatch theory of lateral phase-separation phenomena occurring when the two lipid species have acyl chains differing in their length/number.

Hollars and Dunn [138] showed that bilayers of fluorescently doped DPPC formed by a combination of LB dipping and Langmuir–Schaefer monolayer transfer exhibit complex surface topographies that reflected a convolution of the phase structures present in each of the individual monolayers.

Czajkowsky et al. [139] used TMAFM in the phase shift mode to directly visualize phase-separated lipid bilayers with different surface charge characteristics. A clear correlation was obtained between the direction of the phase shift and the sign of the specimen surface charge. A simple theory was presented, qualitatively consistent with experimental observations.

2.2.3. *Films made of mixtures of lipids with other biomolecules*

Besides mixed lipid films, significant research effort has been put into the study of films composed of mixtures of lipids with other biomolecules such as glycolipids, (lipo)peptides, proteins and cholesterol, with the aim of gaining insight into the miscibility, domain shape and molecular orientation of these compounds. A few investigators have paid attention to lipid/glycolipid mixtures. The distribution of the charged glycolipid ganglioside G_{M1} in phase-separated DOPC/DPPC monolayers transferred on mica was examined by AFM [140]. For concentrations below 1 mol%, G_{M1} distributed exclusively in the LC DPPC phase where it formed nanometer scale patches of round and filamentous shapes both at the boundary and toward the middle of DPPC macrodomains. Raising the concentration increased the number of patches and created fence-like structures at the DOPC/DPPC boundary, while G_{M1} clusters apparently emerged from the LE DOPC phase. Phase-separation was also observed in hydrated bilayers made of a mixture of DOPE and digalactosyldiglyceride (DGDG), a common neutral glycolipid of plant membranes [40].

Several groups have studied mixtures of small (lipo)peptides and phospholipids in supported thin films. Egger et al. [70] reported high resolution images of planar lipid–protein model membranes containing synthetic hybrid molecules consisting of a Fab′ fragment of a monoclonal antibody linked to a phospholipid. LB monolayers composed of a mixture of DPPC and peptide bond bridged phenylalanine–tetraphenylporphyrin were investigated under different surface pressures [141,142]. Phase-separation was noted at pressures higher than 12 mN/m;

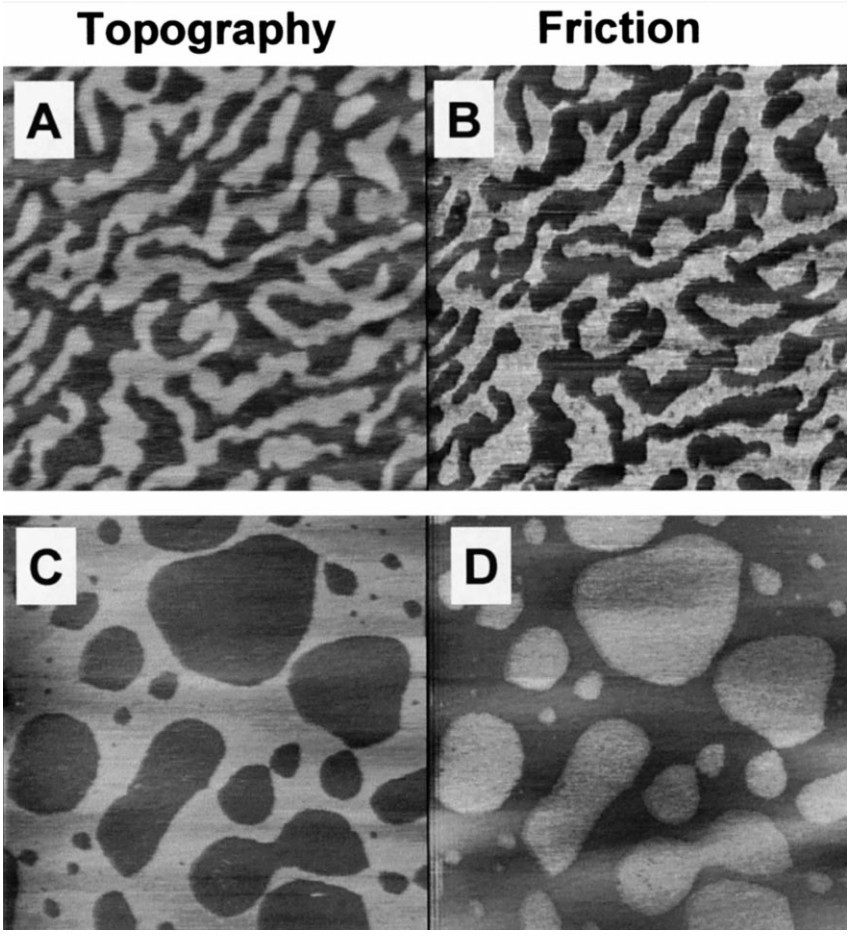

Fig. 5. Topographic (A, C) and friction (B, D) images of mixed (25:75) surfactin/DPPC monolayers in air prepared on a water subphase at pH 2 (A, B; 2×2 μm) and pH 8 (C, D; 5×5 μm).

however, a further increase of surface pressure lead to the squeezing out of DPPC domains from the monolayer.

Vikholm and Peltonen [143] observed mixed DMPC/DMPE monolayers into which a lipid-tagged genetically fragmented antibody was incorporated. These were found to be segregated into protein-rich domains with a mean diameter of about 12 nm.

Dori et al. [144] reported a new method of creating supported bioactive bilayer membranes of either a pure poly(ethylene glycol) (PEG) lipid or 50 mol% binary mixtures of a PEG lipid and a novel collagen-like peptide amphiphile on a hydrophobic surface. The topography of the different systems was analyzed by AFM, most images showing defects with approximately the same coverage. Cell adhesion and spreading assays showed that selective masking of a ligand on a surface is one method of controlling the surface bioactivity.

The aggregation state of gramicidin A, a small channel-forming peptide, in supported PC bilayers was probed in aqueous solution [145]. Gramicidin molecules were found to aggregate into domains composed of small clusters with lipids. The domain size increased with increasing gramicidin concentration. Under certain conditions, multiple lamellar structures showing a ripple-like surface were formed.

To better understand the mechanism involved in the membrane uptake of a vector peptide, the interactions between DOPC and a primary amphipathic peptide were studied with complementary methods [146]. AFM observations of mixed monolayers in air confirmed the existence of phase-separation and further revealed that mixed lipid–peptide particles

are formed, the size and shape of which depend on the peptide molar fraction. Fourier transform infrared spectra obtained on transferred monolayers indicated that the peptide adopts a β-like structure for high peptide molar fractions. In a recent extension of this work [147], where the nature of the phospholipid polar headgroups and alkyl chains was varied, AFM observations showed that the presence of small amounts of peptide led to the appearance of bowl-like particles and that an increase in the peptide amounts generated the formation of filaments. In the case of dioleoylphosphatidylglycerol (DOPG), filaments were found at higher peptide molar fractions than already observed for DOPC because of the presence of negatively charged lipid headgroups.

Surfactin is a surface-active bacterial lipopeptide which is known to have important biological properties, the latter depending on the interaction with lipid membranes. To gain a molecular understanding of this interaction, the nanoscale organization of mixed monolayers of surfactin-C_{15} and DPPC was investigated by AFM and XPS ([41]; Fig. 5). Topographic images of monolayers prepared on a water subphase at pH 2 revealed phase-separation for surfactin molar ratios of 0.1, 0.25 and 0.5, in the form of complex, elongated domains. The step height measured between the surfactin and the DPPC domains was surprisingly high ($\sim$1.2 nm) and a significant contrast in friction was observed. This was attributed to a difference in molecular orientation: while DPPC had a vertical orientation, the large peptide ring of surfactin was lying on the mica surface. Monolayers prepared at pH 8 showed well-defined, round-shaped domains, which were in contrast with the complex shapes observed at pH 2 (Fig. 5); furthermore, the step height measured between the surfactin and the DPPC domains was significantly lower ($\sim$0.8 nm) which could be due to a difference in the molecular orientation of the surfactin alkyl chains. Surface analysis by XPS brought complementary, quantitative information on the spatial organization of the monolayers. Apparent N/C atom concentration ratios were calculated, considering a simple geometric model in which DPPC molecules assume a vertical orientation with the polar head groups in contact with mica while the surfactin peptide rings are lying horizontally. Excellent agreement was found between theoretical and experimental N/C values for various surfactin molar ratios, which directly supported interpretation of the AFM images.

Mixed lipid films containing proteins have also received considerable interest. Mixed monolayers of nicotinic acetylcholine receptor (nAChR) and lipids transferred onto silicon substrates showed the presence of protein aggregates and regular structure in the lipid layer, the sizes of the observed features being consistent with the molecular dimensions of the lipids and nAChR [148].

AFM was used to study the morphology of a pulmonary surfactant model system made of DPPC, dipalmitoylphosphatidylglycerol (DPPG) and recombinant surfactant-associated protein C (SP-C) LB films [149,150]. Phase-separation was demonstrated, in air, in agreement with earlier investigations by fluorescence light microscopy. Smooth polygonal patches of mostly lipid were surrounded by a corrugated rim rich in SP-C. When the films were compressed beyond the equilibrium surface pressure, the protein-rich phase mediated the formation of layered protrusions. The role of SP-C on the structure and dilatational rheological properties of model monolayers of pulmonary surfactant was investigated by Panaiotov et al. [151], using a combination of AFM and rheology measurements. The non-equilibrium effects due to the reorganization of the cluster lipid monolayers increased with increasing protein content. The results confirmed the idea that the hydrophobic pulmonary proteins help to disrupt the bilayers. In another investigation, the structure of pulmonary surfactant films was shown to be heterogeneous, the addition of surfactant proteins inducing web-like protrusions [152].

Kernen et al. [153] imaged monomolecular layers of the largest light-harvesting pigment–protein complex of photosystem II (LHC II), either pure or mixed with lecithin, and revealed ring-like structures suggesting that the protein has a strong tendency to form aggregated structures.

Lin et al. [154] examined the activity of amyloid β protein $A\beta P_{1-40}$ reconstituted in phospholipid vesicles. A combined light fluorescence and atomic force microscope was used to image the structure of reconstituted vesicles and $^{45}Ca^{2+}$ uptake was used as an assay for calcium permeability across the vesicular membrane. The results provided evidence that $A\beta P_{1-40}$ forms calcium-permeable chan-

nels and thus may induce cellular toxicity in Alzheimer's disease.

Finally, Ekelund et al. [155] recently studied lipid mixtures containing cholesterol. Using AFM, they found very small rectangular domains in binary monolayers of synthetic ceramides and cholesterol. When the cholesterol content increased, the domains were bigger although the rectangular shape was retained. The almost perfect shape of the domains indicated two-dimensional single ceramide crystals.

2.3. Supported lipid bilayers as a support for anchoring biomolecules

High resolution imaging of biomacromolecular systems by AFM can only be achieved if they are stably attached to a flat supporting surface [156]. Lipid bilayers supported on flat substrata have proved to be a valuable preparation method in the immobilization of biomolecules (Section 2.3.1) and in the recrystallization of protein arrays (Section 2.3.2) for AFM characterization, thereby providing new insight into structure–function relationships for such biomolecules.

2.3.1. Membrane-bound biomolecules

Weisenhorn et al. [71] reported the use of positively charged lipid bilayers as a substratum to anchor single stranded DNA for high resolution AFM imaging. Using a similar approach, Mou et al. [11] showed that the strong electrostatic interactions between DNA and cationic lipid bilayers resulted in a very stable specimen, enabling direct visualization of the pitch and the right-handed double helix.

Fang and Yang [157] observed that the fluidity of supported cationic lipid membranes promotes the close packing of condensed DNA molecules, independent of the length and shape of the DNA molecule. The 2D condensation required the presence of free DNA molecules in the solution for a period of about 12 h, in which the ratio of adsorbed DNA to the free DNA is about 5% or less. For condensed DNA, the interhelical distance increased with increasing Na^+ concentration. Malghani and Yang [158] found that the height of membrane-bound DNA was the same as the diameter of DNA, indicating no compression by the tip at a probe force of about 0.1 nN; they calculated that the binding strength of DNA molecules to DPPC lipid bilayers should be larger than 2 kT per helical turn.

Polymerized monolayers of diacetylene lipids carrying a metal-chelating headgroup were shown to be a powerful method for the reversible binding of histidine-tagged heat shock factor protein/DNA complexes, as demonstrated by AFM [159].

Clausen-Schaumann and Gaub [160] investigated DNA adsorption to laterally structured charged lipid bilayer patches prepared from vesicle suspensions. DNA adsorption was found to depend on the surface charge density and on the size of the cationic lipid bilayers areas. While on purely cationic lipid bilayers larger than 20 nm a densely packed layer of DNA could be observed, as expected, no DNA could be detected on molecular co-crystals of cationic and anionic lipids where the diameter of the cationic lipid headgroups is only about 0.7 nm. On a 1:1 binary mixture of cationic and neutral lipids, on the other hand, the spacing between adjacent DNA strands was found to double, compared to the purely cationic lipid membranes.

Enzymes embedded in lipid layers have been imaged by AFM, providing valuable information both for technical applications (e.g. the design of biosensors) and for fundamental biomembrane studies. Kasas et al. [161] characterized, under aqueous conditions, the size, form and stability of the plasma membrane Ca^{2+} ATPase, an ATP-driven Ca^{2+} specific pump, reconstituted in asolectin phospholipid liposomes. Using TMAFM in air, Takeyasu et al. [162] analyzed the structure of individual *Escherichia coli* F_0F_1-ATPase and its F_0 sector reconstituted in lipid membranes after staining with uranyl acetate. Singh et al. [163] reported images showing that the native *E. coli* ATP synthase F_0 complex is made of a ring structure surrounding a central dimple. Chloroplast CF_0F_1 ATP synthases reconstituted into liposomes were adsorbed onto mica and imaged in contact mode under physiological conditions [164]. The upper CF_1 part of the enzymes could be removed either by application of a chemical denaturant or by mechanical stripping with the AFM tip. Ring-like structures were observed after mechanical stripping and tentatively attributed to the intrinsic membrane domain CF_0 or the oligomer of its subunit III.

TMAFM images of cytochrome *c* oxidase, the terminal enzyme in oxidative phosphorylation, immobi-

lized within an electrode-supported lipid bilayer membrane revealed that the oxidase is present as monomers and small aggregates within the supported membrane and that the enzyme constitutes 20% of the lipid bilayer membrane [165]. The structural properties of cytochrome *c* LB films were studied on graphite electrode with TMAFM in air [166]. Cytochrome *c* formed ordered monolayers in which the individual proteins packed into a quasi-hexagonal structure. Cytochrome *c* adsorbed spontaneously on cardiolipin monolayers, the adsorbed protein preserving the electron-transfer reaction as probed by cyclic voltammetry. In contrast, no adsorption was observed on PC monolayers. TMAFM in air was applied to study the molecular organization and aggregation states of the hemeprotein cytochrome P450scc, either in pure cytochrome films or in mixed cytochrome/PC films [167]. The topology of the proteins was drastically dependent on surface pressure. The protein appeared to play a role as self-organization centers by adsorbing and orienting the lipid molecules.

Nanobilayers consisting of approximately 10 nm-diameter circular phospholipid domains stabilized by apolipoprotein A1 were used to trap hepatic microsomal NADPH-cytochrome P450 reductase for subsequent AFM imaging [168]. The P450-reductase in the oriented monolayer retained its catalytic activity and isolated single-membrane proteins could be stably imaged over time.

Lipid monolayers deposited onto silicon wafers were fused with liposomes containing acetylcholinesterase and imaged by AFM [39]. The activity of the protein on the solid substrate was verified up to 28 days with a half-life of about 7 days while AFM imaging showed that the topography of the surface did not change significantly during this period.

The structure and function of 20 S proteasome, a macromolecular protease complex, was studied by AFM and SPR [169]. Immobilization to chelator lipid membranes was achieved thanks to engineered histidine tags introduced at defined positions. The overall structure of the proteasome and the organization of individual subunits was resolved under native conditions without fixation or crosslinking. In addition, the substrate–proteasome interaction was monitored in real-time by SPR: the association and dissociation kinetics of the substrate–proteasome complex were analyzed during proteolysis of the polypeptide chain.

Finally, the specific binding of single viruses or proteins to supported lipid bilayers has been reported. Towards the goal of developing biosensors for the detection of viruses, phospholipid bilayers were constructed with 10 mol% of the ganglioside G_{D1a} in the outer monolayer [5]. Specific binding of influenza viruses to G_{D1a} receptors was monitored by AFM and total internal reflection fluorescence. Kolb and Schauer [111] observed, in situ, the binding of anti-TexasRed rabbit IgG antibodies onto mixed lipid bilayers made of phospholipids and TexasRed–sulfonyl-dihexadecanoyl-glycero-phosphoethanolamine.

2.3.2. Crystalline protein arrays

A number of proteins have the ability to form 2D crystalline arrays at lipid surfaces. Electron crystallography has shown to be a powerful approach for determining the structure of these proteins at a near-atomic resolution [8]. The AFM provides complementary information on the molecular structure of protein 2D crystals and makes it possible to monitor conformational changes in real time.

Bacterial cell surface layers (S-layers) are 2D crystalline arrays of (glyco)proteins which can exhibit oblique, square or hexagonal lattice symmetry with spacings of the morphological units in the range 3–30 nm (for reviews, see [170,171]). Isolated S-layer subunits have been reassembled at the surface of phospholipid films [9,172], in an orientation which mimics the surface of the living organisms. S-layers of *Bacillus coagulans* E38–66 and *Bacillus sphaericus* CCM2177 recrystallized on supported DPPE, DMPC and DPPC films have been imaged by AFM in buffer solution [36,172]; they showed oblique and square lattices, respectively, with lattice parameters in agreement with transmission electron microscopy data.

Several proteins crystallize on planar lipid layers through specific interactions, including streptavidin, cholera toxin and annexin V, which bind to negatively charged lipids, biotinylated lipids and gangliosides, respectively (for a recent review, see [8]). Using AFM in real time, the binding of streptavidin proteins to biotinylated lipid bilayers made of mixed DMPE/biotinylated DPPE (19:1) on DPPE-coated

mica was visualized and it was found that streptavidin bound almost exclusively to the biotin in the fluid domains [135,173]. Molecular resolution images of 2D streptavidin crystals transferred on DPPE-coated mica were also reported. Streptavidin crystals grown on biotinylated lipid monolayers at an air/water interface and transferred onto highly oriented pyrolytic graphite could be imaged in buffer solution to a resolution below 1 nm [174].

Yang et al. [73] immobilized crystals of cholera toxin onto cross-linked phospholipid bilayers containing 20 mol% of the glycolipid ganglioside G_{M1}. This procedure allowed the protein to be imaged in aqueous solution at a resolution of 1–2 nm. Later, the same resolution was achieved using a similar approach but without the need for chemical cross-linking [87].

Annexin V specifically binds to negatively charged lipids such as phosphatidylserine (PS) in a Ca^{2+}-dependent manner. The formation of 2D crystals of annexin V onto lipid bilayers was followed in real time by AFM in aqueous environment ([175]; Fig. 6). When the protein was added to PS-containing phospholipid bilayers, circular crystalline domains of micrometer size were formed within 10 min. The submolecular organization of the crystals was characterized at a resolution of $\sim$2 nm. Annexin V trimers were arranged with p6 symmetry, while a seventh trimer was located in a noncrystallographic manner at the six-fold symmetry center. In addition, several types of defects, hitherto not observed in protein crystals, were resolved.

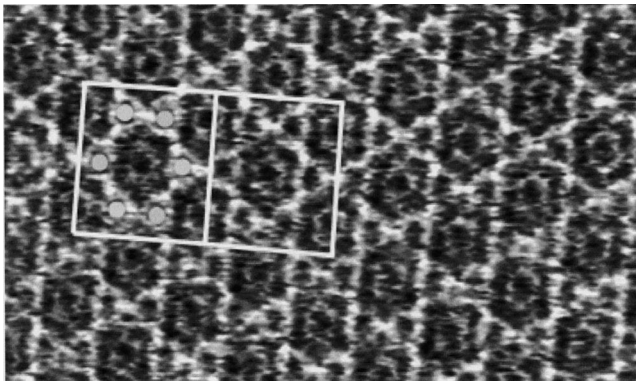

Fig. 6. AFM investigation of the formation of 2D crystals of annexin V onto a PS-containing phospholipid bilayer in aqueous environment. Area size: 200×118 nm. The white box surrounds six trimers (labeled with dots) located at the vertices of a hexagon (courtesy of Professor A. Brisson, University of Groningen, Groningen, The Netherlands).

VacA, a unique protein toxin secreted by the human pathogen *Helicobacter pylori*, was shown to form 2D crystals on planar phospholipid bilayers; hexameric anion selective channels were evidenced using electrophysiological and AFM measurements [176,177].

Fang et al. [178] used AFM to probe the oligomeric state of a genetically engineered mutant of staphylococcal α-hemolysin (α HL-H5) on supported egg-PC (EPC) bilayers. The images showed a heptameric structure for individual oligomers, supporting earlier biochemical determinations. Czajkowsky et al. [179] studied the structure of the α HL oligomer formed in supported phospholipid bilayers. In contrast to X-ray crystallographic data reported for the oligomer in deoxycholate micelles, high resolution AFM images unequivocally revealed a hexamer in these phospholipid bilayers. Independent support of this hexameric stoichiometry was obtained from the measurements of the lattice constant in the AFM images and from gel electrophoresis. AFM has also been used to study self-assembled structures of two α-hemolysin mutants [180]. For the mutant α HL-H5 that was locked into the prepore state on fluid phase EPC membranes, the authors visualized, for the first time, heptameric prepores and showed that the seven-fold axis in the prepore lies perpendicular to the membrane surface. For another mutant (TCM) with the transmembrane domain, the self-assembled oligomer that assumes the conformation of the fully assembled pore was also a heptamer.

Zuber and Barklis [181] visualized, by electron microscopy and AFM, ordered arrays of histidine-tagged Moloney capsid protein (his-MoCA) on membrane bilayers composed of PC and the nickel-chelating lipid 1,2-di-*O*-hexadecyl-*sn*-glycero-3-(1′-2″-*R*-hydroxy-3′*N*-(5-amino-1-carboxypentyl)iminodiacetic acid)propyl ether. AFM images, showing topological features viewed near the membrane proximal domain of the his-MoCA protein, revealed a cage network of symmetrical hexamers spaced at 7.9 nm distances.

Another class of well-ordered crystals consists of protein arrays reconstituted in the presence of lipids, rather than by binding onto lipid bilayers. 2D crystals of porin OmpF, a channel-forming protein of the

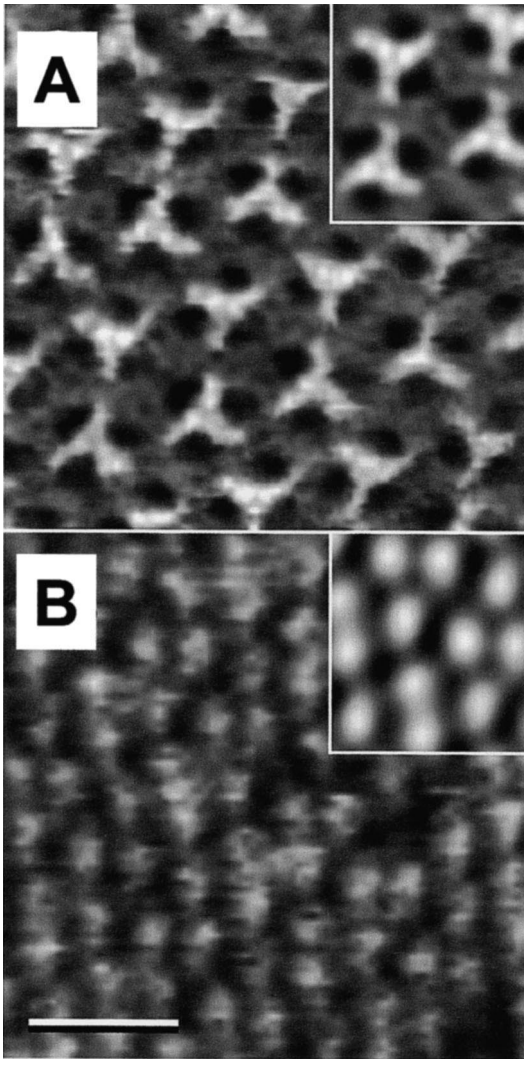

Fig. 7. AFM topographs of the periplasmic (A) and extracellular (B) surface of 2D crystals of the channel forming protein porin OmpF reconstituted in the presence of lipids. Insets: averages calculated from 25 translationally aligned subframes. Scale bar: 10 nm (courtesy of Professor A. Engel, Universität Basel, Basel, Switzerland).

outer membrane of *E. coli*, reconstituted in the presence of lipids, were probed in solution by AFM to a lateral resolution of 1 nm and a vertical resolution of 1 Å ([182]; Fig. 7). Protein–protein interactions were demonstrated on the basis of the AFM results and earlier crystallographic findings. Voltage and pH-dependent conformational changes of the extracellular loops were measured, demonstrating the potential of AFM to monitor conformational changes with high resolution [183].

A second example is aquaporin-1 (AQP1), a membrane channel involved in osmoregulation. Surface AFM topographs confirmed the 3D map of negatively stained AQP1 crystals, which exhibited tetramers with four major protrusions on one side and a large central cavity on the other side of the membrane [184]. Scheuring et al. [185] used AFM to image the surface of aquaporin Z, the water channel of *E. coli*. 2D crystals with p42(1)2 and p4 symmetry were observed. Imaging both crystal types before and after cleavage of the N-termini allowed the cytoplasmic surface to be identified; a drastic change of the cytoplasmic surface accompanied proteolytic cleavage, while the extracellular surface morphology did not change. Flexibility mapping and volume calculations identified the longest loop at the extracellular surface. This loop exhibited a reversible force-induced conformational change.

3. Physical properties

The ability to measure surface forces with nanometer lateral resolution is a unique feature of the AFM. Of primary importance to biomembrane studies, force measurements can be used to characterize the physical, and chemical, properties of lipid layers and their constituents. As we shall see, force measurements also provide a means of understanding the nature of probe–sample interactions, and thus topographic image contrast mechanisms. The following sections introduce the principles of AFM force measurement (Section 3.1), interpretation of these measurements (Section 3.2), and their recent application to supported lipid (Section 3.3) and protein/lipid (Section 3.4) films. Comprehensive reviews of the physical aspects of AFM force measurements have been presented by Butt et al. [186], Burnham et al. [187], Carpick and Salmeron [188], and Cappella and Dietler [189].

3.1. Force measurements by AFM

Interaction forces are measured by monitoring the force applied to the probe as a function of the probe–surface separation. These so-called force curves are typically acquired by monitoring the cantilever displacement (d) as a function of a preselected

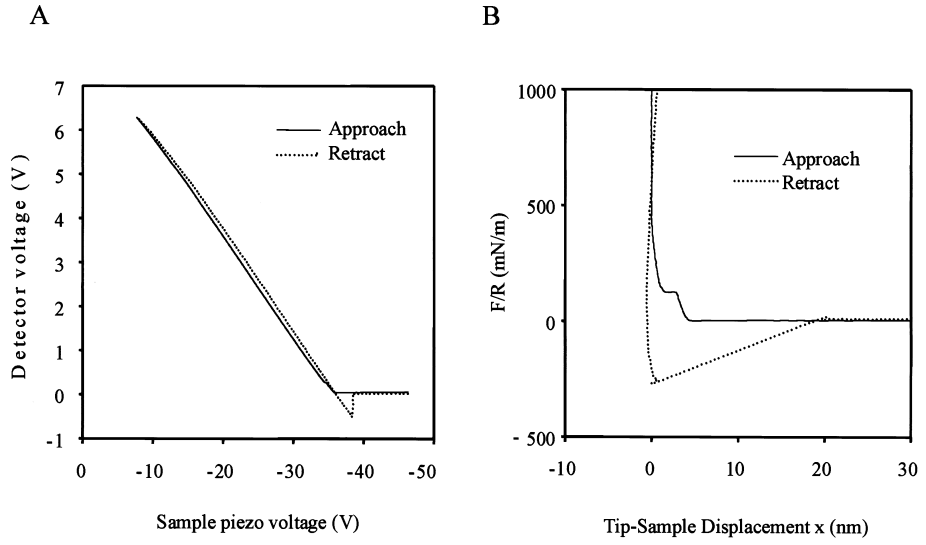

Fig. 8. Detector signal versus sample piezo voltage (A) and normalized force (F/R) versus probe–sample displacement x (B) force curves for probing DSPE bilayers in water with a modified AFM probe. Bold lines are probe approach traces, and dotted lines are retract traces. The raw voltage data were offset to a value of 0 V in the non-contact region of the plot. The data between 2.0 and 4.0 V serve as a calibration regime in which the probe remains at the same depth in the sample.

range of piezo displacement (z, Fig. 8A). This raw data is converted to force (F) versus distance (D) data (Fig. 8B) using Hooke's law $F=-k\Delta d$, where k is the measured spring constant of the cantilever, and the simple geometric relationship $\Delta D=\Delta z-\Delta d$ is used to calculate probe–sample separation. This measurement assumes the probe and surface form a non-deformable contact in the high loading region of the force curve, and lateral motion of the probe across the surface under high loads is negligible. As we shall see, quantitative interpretation of force curves requires careful consideration of each of these assumptions.

Each portion of the force–distance curve produces information about the physical and chemical properties of the sample. The approach portion of the curve can be used to characterize surface properties, such as van der Waals and electrostatic forces [58,59,190], solvation [191,192] and hydration [58,193], and steric/bridging forces associated with polymer-covered surfaces [57]. Once the cantilever is in contact, the shape of the approach curves may provide direct information on the mechanical properties of the samples [194,195]. The retraction force curves often show a hysteresis referred to as the adhesion 'pull-off' force, which can be used to estimate the surface energy of solids [54,194,196].

The force measurement technique described above is widely used to characterize surface forces because of its simplicity and compatibility with commercial AFM imaging instruments. Several other force techniques have been developed to measure force more quantitatively. Among the most exciting developments has been magnetic force feedback [197]. In a recent demonstration [198], this technique was used to measure the interatomic potential between a silicon probe–substrate, demonstrating that the additivity of interatomic potentials is not valid at this scale. This technique has also been applied to the study of the molecular nature of fluid–surface interactions [199] and the mechanical properties of single biopolymers [200]. Force can also be measured by monitoring the resonance frequency of the cantilever as a function of probe–surface separation [201]. Resonance force sensing has primarily been used for characterizing the mechanical properties of soft materials such as polymer blends [202–204], although it can also be used to sense surface forces [139,205]. Finally, probe–surface interaction forces are indirectly sensed in the lateral force imaging mode [53], and can be

qualitatively interpreted if the probe chemistry is defined [54].

3.2. Interpretation of force measurements

A probe–sample interaction is dependent on the geometry and chemistry of the probe and substrate, and on the nature of the intervening medium. Many AFM studies have qualitatively characterized the properties of a surface at the nanometer scale using force. However, if the probe and environmental properties are defined, force may be used to determine the surface charge density, Hamaker constant and elastic modulus of the surface. Here, we describe how the geometry and chemistry of the probe can be determined, and develop a theoretical framework in which a force curve can be interpreted.

Most contact imaging is done with silicon oxynitride microfabricated probes that have a nominal radius of curvature of 25 nm [206]. These probes have a surface morphology that cannot be controlled at the nanometer scale. However, the development of nanofaceted crystals has made it possible to characterize probe geometries with nanometer resolution in minutes [207]. The silicon oxynitride surface is composed of ionizable silanol and silylamine groups that vary in density with pH, which is further complicated by the fact that microfabrication results in contamination by gold and other materials [208,209]. To overcome this limitation, different approaches have been developed to create probes of well-defined chemistry. The first approach was to attach a micron-size particle such as a silica microsphere to the cantilever [57,59]. These spheres were subsequently coated with silanes [210] and biopolymers [60,61]. Although this approach provides well-defined surface chemistries, it cannot be used for imaging with high lateral resolution. Functionalizing sharp AFM probes with SAMs of organic alkanethiols combines the advantage of strong chemical sensitivity with high spatial resolution [54]. This procedure involves coating microfabricated cantilevers with a thin adhesive layer (Cr or Ti), followed by a 15–100 nm thick Au layer and immersing the coated cantilevers in dilute (0.1–1 mM) ethanol solutions of the selected alkanethiol. This approach produces modified probes that are chemically stable and mechanically robust; furthermore, thiols with a variety of terminal functionalities can be used, allowing different types of surface forces or physicochemical properties to be investigated. Recently, covalent modification of nanotube probes has been used to measure molecular interactions at biological interfaces with unprecedented lateral resolution [211,212].

Force as measured with the AFM is a dependent variable. This means that a measurement made with an AFM probe cannot be directly related to other force or thermodynamic measurements. If interatomic potential additivity is assumed, an analytical expression can be developed to convert the force between a sphere and flat F_s to energy per unit area between parallel planes E_p:

$$F_s(D)/R = 2\pi E_p(D) \quad (1)$$

where D is the distance between the surfaces and R is the radius of curvature of the probe [213]. Derjaguin's approximation applies only to measurements in which the range of the interaction and D are much smaller than R. This approximation has been recently applied to the measurement of short-range repulsive hydration/steric and van der Waals forces between uncharged lipid bilayers and thiol-functionalized probes of defined geometry [214]. $F_s(D)/R$ was found to be independent of radii for 25 nm $< R <$ 100 nm.

For long-range forces (e.g. electrostatic and steric interactions), the validity of Derjaguin's approximation and the conical shape of the AFM probe may become an issue. Electrostatic force between probes and surfaces of varying charge has been measured in solutions of defined ionic strength [58,215,216]. Although the radius of curvature of the probe was not directly measured, the surface potential was computed using an expression for electrostatic force derived from the Poisson–Boltzmann equation and Derjaguin's approximation. The surface potential of several inorganic materials was consistent with the expected values. Application of this approximation to electrostatic forces appears to be valid if $R \gg \kappa^{-1}$, where κ^{-1} is the Debye length [217,218].

Mechanical properties dominate the measured AFM forces once a probe makes contact with a surface. The nanometer scale mechanical properties of supported lipid films have been studied in air and water. In air, liquid crystalline DSPE, MGDG and DGDG monolayers behaved elastically and the form

of load–displacement curves appeared to be consistent with Hertzian contact mechanics [133]. Hertz's model relates the δ deformation of a film to load P for a probe radius R:

$$\delta = (9P^2/16RE^{*2})^{1/3} \quad (2)$$

where $E^* = [(1-v_1^2)/E_1 + (1-v_2^2)/E_2]$ and E_1, v_1, and E_2, v_2 are Young's modulus and Poisson's ratio of the probe and sample, respectively [219]. Liquid expanded DOPE monolayers were highly inelastic and non-Hertzian.

In water, the mechanical properties of the two layers of the supported bilayer were found to vary significantly. Hertzian analysis of the initial load–deformation behavior of the layer facing the aqueous phase produced a Young's modulus consistent with the isothermal thickness compression modulus of the monolayers measured during LB deposition [40]. Larger indents resulted in an abrupt rupture of the outer monolayer. The monolayer facing the supporting surface appeared to interact with the mica substrate and the mechanical properties were dominated by the underlying mica substrate.

Adhesion is a parameter related to the chemical properties of the interface, which is highly relevant to many biological processes. Nanometer scale adhesion of monolayer films on hard surfaces in air has been studied due to its relevance to boundary layer lubrication [220]. Recently, AFM surface force measurements were made on DSPE, DGDG and MGDG lipid films with functionalized probes of defined radius, and a strong adhesive force was observed on all monolayers under high loading conditions [221]. Using macroscopic contact mechanics, the pull-off force $(F/R)_0$ is related to the work of adhesion (W) between the probe and sample:

$$W = \frac{2}{\chi\pi}\left(\frac{F}{R}\right)_0 \quad (3)$$

where χ is either 3 or 4 for JKR or DMT mechanics, respectively [219]. The JKR theory extends Hertz's theory to account for the creation of additional contact area due to adhesive forces, and the DMT theory extends JKR theory to explicitly account for the finite range of surface forces at the edge of the contact region. Surface force measurements on all lipid films with hexadecanethiol functionalized probes and analyzed with DMT theory produced a work of adhesion ranging between 60 and 90 mJ/m^2, which agrees well with the work of adhesion calculated for alkyl chains in water. Smaller work of adhesion was measured between 16-hydroxyhexadecanethiol functionalized probes and the monolayers, which is consistent with a decrease in the surface energy of the system.

This section has reviewed the analysis of probe–lipid surface interactions based on a continuum approach. As more quantitative force measurements become available for complex systems, we anticipate that the molecular nature of the probe–surface interaction will need to be considered and a more sophisticated treatment of force will be required. Specifically, molecular dynamics simulations will play an import role in future studies.

3.3. Application to supported lipid films

Surface forces associated with lipid films have attracted much attention because of their key role in determining cellular phenomena such as molecular recognition, cell adhesion, cell fusion and intercellular communication. Although the forces between lipid membranes have been widely studied using the osmotic stress method [222], the surface force apparatus [223] and the micropipet technique [224], direct information at high lateral resolution was inaccessible. AFM offers the unique opportunity to probe local physical properties and interaction forces of lipid bilayers with nanoscale lateral resolution, thereby providing new insight into the molecular mechanisms of cell adhesion and membrane fusion.

Force–distance curves have been used to characterize the surface properties of heterogeneous lipid monolayers in air. Adhesion maps were recorded for DMPE monolayers exhibiting coexisting LE/LC phases [225]. The observed adhesion contrast was attributed to differences in the surface energies of the two phases. Knapp et al. [96] used hydrophobic probes prepared by glow discharge in a hexafluoropropene atmosphere to record force–distance curves over the different layers of DPPC/DPPE multilayer systems in air; this allowed the hydrophilic/hydrophobic character of each layer to be identified. Force–distance curves recorded over phase-separated DSPE/DOPE monolayers in air showed adhesive forces ([133]; Fig. 9B) that were clearly larger over

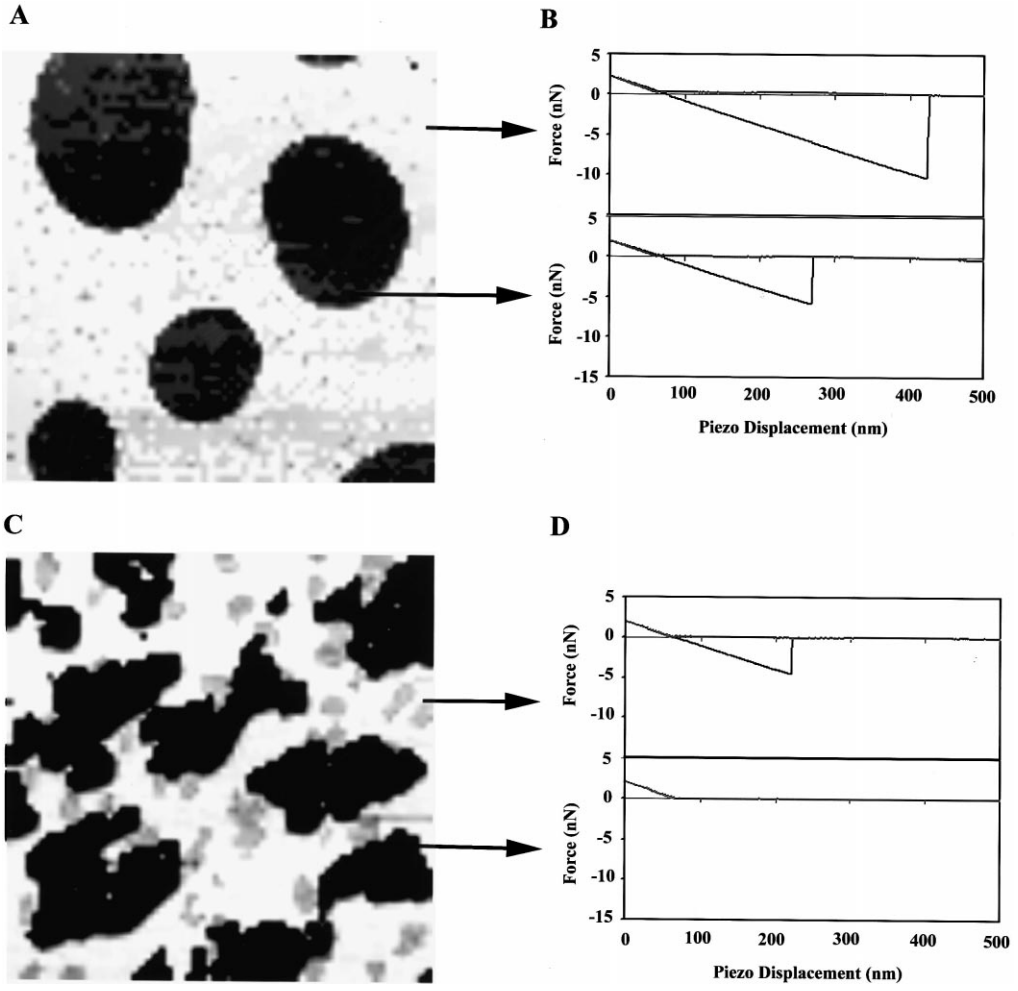

Fig. 9. Adhesion force mapping (15×15 μm areas) of mixed DSPE/DOPE monolayers in air (A, B) and bilayers under water (C, D), using silicon nitride AFM probes.

the liquid-like DOPE domains (10 nN) than over the solid-like DSPE domains (6 nN). As a result, adhesion maps generated by recording multiple force–distance curves showed a high contrast (Fig. 9A). The difference in adhesion was directly correlated to the friction contrast (Fig. 4) and attributed to the mechanical responses of the two lipid phases.

The film mechanical properties were investigated further by measuring the thicknesses of DSPE and DOPE monolayers as a function of applied load after scraping the monolayer away with the AFM probe in a defined area [133]. The two lipid films exhibited very different behaviors: while the DSPE layer was gradually compressed with increasing loads, in agreement with an elastic model, the apparent thickness of the DOPE layer was small and did not change significantly with the applied load, suggesting the film was inelastically deformed as a result of low intermolecular cohesive forces. This difference in the film mechanical properties significantly increased the step height measured at the DSPE/DOPE phase boundary (Fig. 4).

The forces acting at the surface of various lipid bilayers were characterized under aqueous conditions. Ducker and Clarke [226] measured the normal and lateral (friction) forces between silicon nitride surfaces in water, in the presence and absence of the diheptanoic-*sn*-glycero-3-phosphocholine. Adsorption of lipid bilayers caused a large reduction of attractive forces and lateral forces, and produced a short-range repulsion attributed to hydration/steric forces. Furthermore, a cantilever instability occurred

at high loads (>2 nN), which was suggested to result from the squeezing out of the adsorbed lipid bilayer. Rotsch and Radmacher [227] measured electrostatic interactions between a silicon nitride probe and a chemically heterogeneous surface made of positively charged amphiphilic bilayer patches adsorbed onto negatively charged mica. They demonstrated how a force map can be processed to display, with a lateral resolution of 25 nm, the adhesion force as well as the apparent strength and decay length of the electrostatic interaction. Although significant adhesion was detected on the bilayer, there was virtually no adhesion on mica. The electrostatic interaction was attractive on the bilayer patch and repulsive on mica and was affected by the nature and concentration of electrolytes. Force–distance curves and LFM were used to characterize supported planar lipid bilayers prepared by microcontact printed lipophilic SAMs [228]. When lipid vesicles interacted with patterned SAM surfaces, an inversion of friction and adhesion contrast was observed under water, which was related to a difference in the film mechanical properties. The magnitude of the adhesion force measured over the lipid surface with octadecanethiol modified probes was smaller compared to that found with silicon nitride probes.

Force–distance curves recorded over phase-separated DSPE/DOPE bilayers in water depended strongly on the molecular packing of the two phospholipids (Fig. 9): upon retraction, the liquid-like DOPE phase showed a strong adhesive pull-off force (~ 5 nN), while there was no adhesion on the solid-like DSPE domains (Fig. 9D), yielding a highly contrasted adhesion image (Fig. 9C) [133]. This provided direct evidence for the influence of the structure of lipid bilayers on their interaction forces, an effect that may be of prime importance in the control of cellular interactions.

In addition, repulsive forces were observed at the surface of DSPE on approach. The nature of these forces was investigated further using AFM probes functionalized with alkanethiol SAMs terminated with hydroxyl groups [40]. The repulsion force measured over the DSPE domains was well-fitted with models that combined both hydration/steric forces and mechanical deformation, highlighting the important role that mechanics may play in biomolecular interactions. As the load was increased (>10 nN), mechanical deformation played an increasingly important role, until a breakthrough event was observed indicating penetration of the probe through the bilayer. Similar results were obtained when DSPE was replaced by the glycolipid, DGDG.

Recently, the effect of imaging load on the topographic and friction image contrasts of phase-separated lipid bilayers in water was investigated, to clarify the image contrast mechanisms ([214]; Fig. 10). Topographic images of mixed DSPE/DOPE monolayers on DSPE-coated mica showed high contrast at imaging loads below $F/R = 105$ mN/m, while the contrast was completely removed above $F/R = 220$ mN/m. The imaging contrast was recovered when reapplying forces below $F/R = 105$ mN/m, little damage to the films being caused by the high load imaging. Strikingly, the frictional contrast observed at low loads was inverted and magnified at high loads, even when the topographic contrast vanished. Comparison of force curves and topography across domains shows that the source of contrast is a selective breakthrough of one domain between the breakthrough force of each phase (Fig. 10E). It was therefore recommended that force–distance curve analysis be performed prior to imaging any new multicomponent lipid film to determine the load appropriate for the desired imaging contrast.

Charged phospholipids were used to functionalize AFM probes and measure forces on various samples under aqueous conditions [229]. The adhesion force between the charged probes and oppositely charged specimens was much larger than when uncoated probes were used; this was attributed to salt bridge formation. The colloidal probe method has been used to measure forces between LB films of metal-chelating lipids in water [230]. The electrostatic interactions were measured between monolayers of lipids functionalized by the iminodiacetic acid group transferred on hydrophobic glass substrates. The double layer repulsion between the films changed with pH, reflecting the different protonation states of the iminodiacetic acid groups. Cu^{2+} complexation was also monitored by measuring the force profiles at various Cu^{2+} ion concentrations.

It is worth noting that besides force–distance curve measurements, new imaging modes are being used to probe the mechanical properties of lipid films. Hollars and Dunn [126] used tapping-mode NSOM

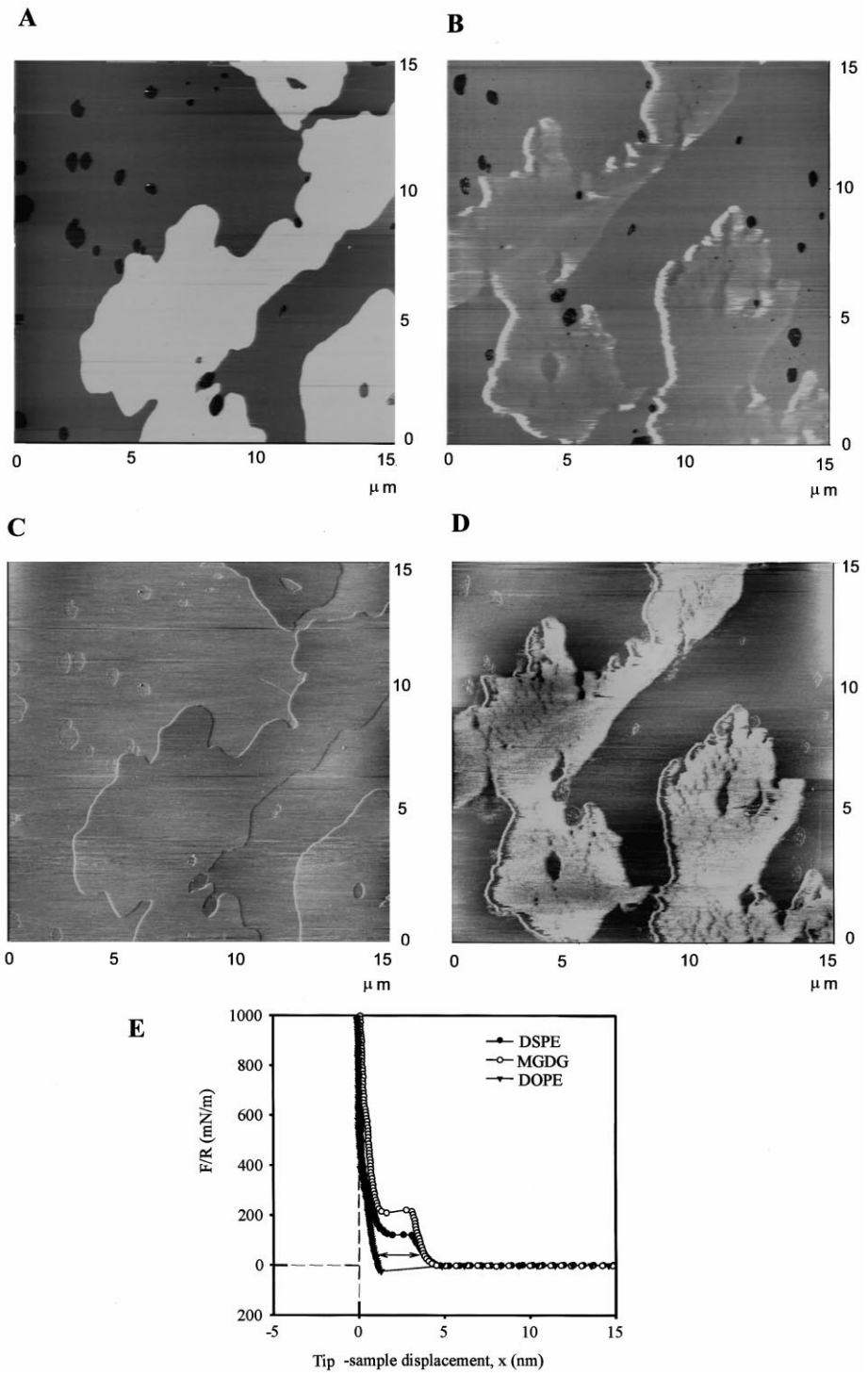

Fig. 10. Effect of imaging load on the topographic (A, C) and friction (B, D) image contrasts of mixed DSPE/DOPE monolayers on DSPE-coated mica: imaging loads smaller (A, B) and larger (C, D) than the breakthrough force ($F/R = 105$ mN/m); normalized force–distance curves recorded over the DSPE and DOPE domains (E).

(TM-NSOM) to probe the compliance properties of phase-separated DPPC lipid monolayers doped with fluorescent dye and deposited in the solid condensed/liquid condensed coexistence region. By monitoring the phase of the TM-NSOM tip resonance, the authors showed that the two lipid phases exhibited distinctly different mechanical properties, the liquid phase domains being more compliant than the surrounding solid phase.

Heinz and Hoh [231], have developed an imaging mode called D minus D (D−D) that uses a change in ionic strength to separate surface charge from morphology in images. Although surface charge is not quantitatively measured, this technique has the advantage of being independent of tip–sample contact point, cantilever spring constant, tip radius and tip surface charge density. D−D images of stacked DPPS bilayers show no charge contrast; images of DPPC bilayers on mica demonstrate contrast due to charge density differences; and images of bacteria rhodopsin membranes on mica show the membranes have a higher surface charge density than mica.

The interaction of DMPC-coated silicon surfaces prepared from vesicle suspensions was investigated with an AFM in an electrolyte solution [232]. A long-range interaction was observed, even when the surfaces were covered with nominally neutral lipid layers. The interaction was attributed to Coulomb interactions of charges located at the lipid surface. The experimental force curves were compared with solutions for the linearized as well as with exact solutions of the Poisson–Boltzmann equation. The comparison suggested that, in 0.5 mM KCl electrolyte, the DMPC lipids carried about one unit of charge per 100 lipid molecules. The presence of this surface charge made it impossible to observe an effective charge density recently predicted for dipole layers near a dielectric when immersed in an electrolyte. A discrepancy between the theoretical results and the data at short separations was interpreted in terms of a decrease in the surface charge with separation distance.

3.4. Application to protein/lipid films

Measurements of physical properties have not been restricted to pure lipid films but are being more and more extended to protein–lipid systems. Force–distance curves were recorded, at different pH values, on purple membranes adsorbed to alumina using silicon nitride probes [233]. At high pH (8–10), the approach curves showed long-range repulsion due to electrostatic repulsive forces between negatively charged surfaces. When the pH was lowered, the repulsion range decreased. By comparing the forces measured on both purple membranes and bare alumina, the surface charge density of the former was estimated to be -0.05 C/m^2. The surface potential of the crystal surface could be determined, and the isoelectric point was found to be about 4.

Müller et al. [234] recorded force–distance curves, at different electrolyte concentrations, between silicon nitride probes and the surface of purple membranes and OmpF porins. In the presence of 20 mM KCl, long-range repulsion forces were measured, reflecting the electrostatic double-layer repulsion. The authors estimated the pH and electrolyte concentration required to adjust the double-layer repulsion so that both vertical and lateral forces are minimized, thereby improving the spatial resolution.

Force–distance curves were recorded between the S-layers of *B. sphaericus* CCM2177 and of *B. coagulans* E38–66 and methyl-terminated probes [235]. The curves always showed repulsive forces on approach and no adhesion on retraction. The repulsive forces decayed exponentially with distance, with characteristic ranges of $\sim$50 nm for *B. sphaericus* CCM2177 and $\sim$10 nm for *B. coagulans* E38–66. Similar results were obtained with hydroxyl-terminated probes. The observed non-adhesive properties may play an important role in determining the biological function of S-layers.

Mueller et al. [236] recently took advantage of the AFM to gain insight into the physicochemical basis of the myelination process in which two opposed membranes adhere in the presence of myelin basic protein (MBP). To this end, probe–sample interaction of mica and mixed DOPS (20%)/EPC (80%) lipid bilayer surfaces were measured in the absence and presence of bovine MBP. While on mica or DOPS/EPC bilayers, a short-range repulsive force (decay length of 1.0–1.3 nm) was observed during the approach, the presence of MBP always led to an attractive force between probe and sample, consistent with the MBP ascribed role of compacting apposed membranes in myelin. MBP molecules at-

tached to the mica surface exhibited elastic stretching behavior that agreed with the worm-like chain model. However, MBP attached to a lipid bilayer did not show elastic stretching, suggesting that the protein adopts a different conformation when in contact with lipids.

4. Conclusions

The first AFM images revealing the molecular structure of supported phospholipid films were reported in 1990 [70]. Since then, a broad spectrum of AFM applications have emerged in model membrane biophysics, allowing the study of the structure and function of biomembranes and of biological processes such as molecular recognition, enzymatic activity, cell adhesion processes. More specifically, the instrument has been widely used to characterize the molecular structure of a variety of supported lipid films, the formation of structural defects, the effect of external agents on film structure, the organization of phase-separated films (coexistence region, mixed films), and biomolecules such as DNA, enzymes and crystalline protein arrays anchored to supported lipid bilayers. While considerable progress has been made in AFM instrumentation and preparation techniques, providing now routine images with subnanometer resolution, it must be kept in mind that image interpretation often remains challenging due to the many factors that influence their formation (surface morphology, physical properties, imaging parameters and probe characteristics). We have emphasized the importance of considering force and mechanics while imaging lipid films in order to understand the image contrast mechanisms.

Force–distance curves have provided new insight into the physical properties of lipid films: surface forces (hydration/steric, van der Waals, electrostatic forces), nanomechanics and adhesion. Quantitative interpretation of force measurements requires separation of the relative contributions of the different effects that contribute to the measured forces. This can be achieved by controlling the geometry and chemistry of the probe and applying appropriate theoretical treatments. So far, the analysis of probe–sample interactions in lipid film systems has been described on the basis of a continuum approach. As quantitative force measurements will become available for complex systems and the scale of measurement will drop below 10 nm, we may anticipate that the molecular nature of the interaction will have to be considered and that more sophisticated treatment of forces will be required. In particular, we believe that molecular dynamics simulations will play an important role in future lipid film studies, as is already the case in the emerging field of 'single-molecule force spectroscopy' [237].

Acknowledgements

The support of the National Foundation for Scientific Research (FNRS), the Federal Office for Scientific, Technical and Cultural Affairs (Interuniversity Poles of Attraction Programme), the Office of Naval Research and the Purdue Research Foundation is gratefully acknowledged. The authors would like to thank W. Barger, M. Deleu, J. Green, M. Paquot and J. Schneider for fruitful collaborations and valuable discussions.

References

[1] H. Bader, B. Schlarb, H. Ringsdorf, Adv. Polym. Sci. 64 (1984) 1–62.
[2] H.M. McConnell, T.H. Watts, R.M. Weis, A.A. Brian, Biochim. Biophys. Acta 864 (1986) 95–106.
[3] E. Sackmann, Science 271 (1996) 43–48.
[4] N.L. Thompson, A.G. Palmer, Comments Mol. Cell. Biophys. 5 (1988) 39–56.
[5] L.K. Tamm, C. Böhm, J. Yang, Z. Shao, J. Hwang, M. Edidin, E. Betzig, Thin Solid Films 813 (1996) 284–285.
[6] I. Vikholm, E. Györvary, J. Peltonen, Langmuir 12 (1996) 3276–3281.
[7] A. Brisson, A. Olofsson, P. Ringler, M. Schmutz, S. Stoylova, Biol. Cell. 80 (1994) 221–228.
[8] A. Brisson, W. Bergsma-Schutter, F. Oling, O. Lambert, I. Reviakine, J. Cryst. Growth 196 (1999) 456–470.
[9] D. Pum, M. Weinhandl, C. Hödl, U.B. Sleytr, J. Bacteriol. 175 (1993) 2762–2766.
[10] H.O. Ribi, D.S. Ludwig, K.L. Mercer, G.K. Schoolnik, R.D. Kornberg, Science 239 (1988) 1272–1276.
[11] J. Mou, D.M. Czajkowsky, Y. Zhang, Z. Shao, FEBS Lett. 371 (1995) 279–282.
[12] G.L. Gaines, Jr., Insoluble Monolayers at Liquid–Gas Interfaces, Interscience Publishers, New York, 1966.
[13] A. Ulman, J. Mater. Educ. 11 (1989) 205–280.

[14] K.A. Blodgett, I. Langmuir, Phys. Rev. 51 (1937) 964–982.
[15] L.K. Tamm, H.M. McConnell, Biophys. J. 47 (1985) 105–113.
[16] A.A. Brian, H.M. McConnell, Proc. Natl. Acad. Sci. USA 81 (1984) 6159–6163.
[17] J. Mou, J. Yang, Z. Shao, Biochemistry 33 (1994) 4439–4443.
[18] J. Mou, J. Yang, C. Huang, Z. Shao, Biochemistry 33 (1994) 9981–9985.
[19] E. Kalb, S. Frey, L.K. Tamm, Biochim. Biophys. Acta 1103 (1992) 307–316.
[20] B.A. Cornell, V.L.B. Braach-Maksvytis, L.G. King, P.D.J. Osman, B. Ragues, L. Wieczorek, R.J. Pace, Nature 387 (1997) 580–583.
[21] E.-L. Florin, H.E. Gaub, Biophys. J. 64 (1993) 375–383.
[22] C.W. Meuse, S. Krueger, C.F. Majkrzak, J.A. Dura, J. Fu, J.T. Connor, A.L. Plant, Biophys. J. 74 (1998) 1388–1398.
[23] A.L. Plant, Langmuir 9 (1993) 2764–2767.
[24] A.L. Plant, Langmuir 15 (1999) 5128–5135.
[25] S.-P. Heyn, M. Egger, H.E. Gaub, J. Phys. Chem. 94 (1990) 5073–5078.
[26] H. Möhwald, Thin Solid Films 159 (1988) 1–15.
[27] J.P. Slotte, Biochim. Biophys. Acta 1235 (1995) 419–427.
[28] E. Györvary, W.M. Albers, J. Peltonen, Langmuir 15 (1999) 2516–2524.
[29] D. Hönig, D. Möbius, J. Phys. Chem. 93 (1991) 4590–4592.
[30] S.Y. Zaitsev, V.P. Zubov, D. Möbius, Colloid Surf. A: Physicochem. Eng. Asp. 94 (1995) 75–83.
[31] H. Baltes, M. Schwendler, C.A. Helm, H. Möhwald, J. Colloid Interface Sci. 178 (1996) 135–143.
[32] K. Kago, H. Matsuoka, R. Yoshitome, H. Yamaoka, K. Ijiro, M. Shimomura, Langmuir 15 (1999) 5193–5196.
[33] B.W. Koenig, S. Krueger, W.J. Orts, C.F. Majkrzak, N.F. Berk, J.V. Silverton, K. Gawrisch, Langmuir 12 (1996) 1343–1350.
[34] H. Reinl, T. Brumm, T.M. Bayerl, Biophys. J. 61 (1992) 1025–1035.
[35] D. Axelrod, D.E. Koppel, J. Schlessinger, E. Elson, W.W. Webb, Biophys. J. 16 (1976) 1055–1069.
[36] E. Györvary, B. Wetzer, U.B. Sleytr, Langmuir 15 (1999) 1337–1347.
[37] V. Schram, H.-N. Lin, T.E. Thompson, Biophys. J. 71 (1996) 1811–1822.
[38] W.L.C. Vaz, E.C.C. Melo, T.E. Thompson, Biophys. J. 56 (1989) 869–876.
[39] P.A. Ohlsson, T. Tjärnhage, E. Herbai, S. Löfas, G. Puu, Bioelectrochem. Bioenerg. 38 (1995) 137–148.
[40] Y.F. Dufrêne, T. Boland, J.W. Schneider, W.R. Barger, G.U Lee, Faraday Discuss. 111 (1998) 79–94.
[41] M. Deleu, M. Paquot, P. Jacques, P. Thonart, Y. Adriaensen, Y.F. Dufrêne, Biophys. J. 77 (1999) 2304–2310.
[42] R. Linton, V. Guarisco, J.J. Lee, B. Hagenhoff, A. Benninghoven, Thin Solid Films 210/211 (1992) 565–570.
[43] S. Matuoka, H. Asami, I. Hatta, T. Ishii, K. Yoshikawa, Thin Solid Films 180 (1989) 123–127.
[44] J.M. Solletti, M. Botreau, F. Sommer, W.L. Brunat, S. Kasas, T.M. Duc, M.R. Celio, Langmuir 12 (1996) 5379–5386.
[45] K.M. Leufgen, H. Rulle, A. Benninghoven, M. Sieber, H.-J. Galla, Langmuir 12 (1996) 1708–1711.
[46] G. Binnig, C.F. Quate, Ch. Gerber, Phys. Rev. Lett. 56 (1986) 930–933.
[47] D. Baselt, The Tip–Sample Interaction in Atomic Force Microscopy and its Implications for Biological Applications, Ph.D. thesis, 1993.
[48] D.A. Bonnell, Scanning Tunneling Microscopy and Spectroscopy: Theory, Techniques and Applications, VCH, New York, 1993.
[49] G.J. Leggett, in: J.C. Vickerman (Ed.), Surface Analysis: the Principal Techniques, Wiley, Chichester, 1997, pp. 393–449.
[50] S.N. Magonov, M.-H. Whangbo, Surface Analysis with STM and AFM, VCH, New York, 1996.
[51] E. Meyer, Prog. Surf. Sci. 41 (1992) 3–49.
[52] R. Wiesendanger, Scanning Probe Microscopy and Spectroscopy: Methods and Applications, Cambridge University Press, Cambridge, 1994.
[53] C.M. Mate, G.M. McClelland, R. Erlandsson, S. Chiang, Phys. Rev. Lett. 59 (1987) 1942–1945.
[54] C.D. Frisbie, L.F. Rozsnyai, A. Noy, M.S. Wrighton, C.M. Lieber, Science 265 (1994) 2071–2074.
[55] O. Marti, Phys. Scr. T49B (1993) 599–604.
[56] R.M. Overney, E. Meyer, J. Frommer, D. Brodbeck, R. Lüthi, L. Howald, H.-J. Güntherodt, M. Fujihira, H. Takano, Y. Gotoh, Nature 359 (1992) 133–135.
[57] S. Biggs, Langmuir 11 (1995) 156–162.
[58] H.-J. Butt, Biophys. J. 60 (1991) 1438–1444.
[59] W.A. Ducker, T.J. Senden, R.M. Pashley, Nature 353 (1991) 239–241.
[60] G.U Lee, D.A. Kidwell, R.J. Colton, Langmuir 10 (1994) 354–357.
[61] G.U Lee, L.A. Chrisey, R.J. Colton, Science 266 (1994) 771–773.
[62] M. Rief, F. Oesterhelt, B. Heymann, H.E. Gaub, Science 275 (1997) 1295–1297.
[63] N.A. Burnham, R.J. Colton, H.M. Pollock, Nanotechnology 4 (1993) 64–80.
[64] M. Radmacher, R.W. Tillmann, H.E. Gaub, Biophys. J. 64 (1993) 735–742.
[65] E. Nagao, J.A. Dvorak, Biophys. J. 76 (1999) 3289–3297.
[66] Q. Zong, D. Innis, K. Kjoller, V.B. Elings, Surf. Sci. Lett. 290 (1993) L688–L692.
[67] H.G. Hansma, J.H. Hoh, Annu. Rev. Biophys. Biomol. Struct. 23 (1994) 115–139.
[68] A. Ikai, Surf. Sci. Rep. 26 (1996) 261–332.
[69] Z. Shao, J. Mou, D.M. Czajkowsky, J. Yang, J.-Y. Yuan, Adv. Phys. 45 (1996) 1–86.
[70] M. Egger, F. Ohnesorge, A.L. Weisenhorn, S.P. Heyn, B. Drake, C.B. Prater, S.A.C. Gould, P.K. Hansma, H.E. Gaub, J. Struct. Biol. 103 (1990) 89–94.
[71] A.L. Weisenhorn, M. Egger, F. Ohnesorge, S.A.C. Gould,

S.-P. Heyn, H.G. Hansma, R.L. Sinsheimer, H.E. Gaub, P.K. Hansma, Langmuir 7 (1991) 8–12.
[72] J.A.N. Zasadzinski, C.A. Helm, M.L. Longo, A.L. Weisenhorn, S.A.C. Gould, P.K. Hansma, Biophys. J. 59 (1991) 755–760.
[73] J. Yang, L.K. Tamm, T.W. Tillack, Z. Shao, J. Mol. Biol. 229 (1993) 286–290.
[74] S.W. Hui, R. Viswanathan, J.A. Zasadzinski, J.N. Israelachvili, Biophys. J. 68 (1995) 171–178.
[75] C. Yuan, X. Yang, Z. Lu, J. Liu, Surf. Sci. 355 (1996) L381–L384.
[76] U. Muscatello, G. Valdrè, U. Valdrè, J. Microsc. 182 (1996) 200–207.
[77] S.M. Stephens, R.A. Dluhy, Thin Solid Films 284/285 (1996) 381–386.
[78] H. Iwamoto, N. Wakayama, Jpn. J. Appl. Phys. 36 (1997) 3913–3916.
[79] X. Zhai, J.M. Kleijn, Thin Solid Films 304 (1997) 327–332.
[80] Y. Chunbo, L. Zuhong, L. Juzheng, W. Ying, Prog. Nat. Sci. 7 (1997) 494–498.
[81] J. Garnaes, D.K. Schwartz, R. Viswanathan, J.A.N. Zasadzinski, Nature 357 (1992) 54–57.
[82] H.G. Hansma, S.A.C. Gould, P.K. Hansma, H.E. Gaub, M.L. Longo, J.A.N. Zasadzinski, Langmuir 7 (1991) 1051–1054.
[83] E. Meyer, L. Howald, R.M. Overney, H. Heinzelmann, J. Frommer, H.-J. Güntherodt, T. Wagner, H. Schier, S. Roth, Nature 349 (1991) 398–400.
[84] D.K. Schwartz, J. Garnaes, R. Viswanathan, J.A. Zasadzinski, Science 257 (1992) 508–511.
[85] J.A. Zasadzinski, R. Viswanathan, L. Madsen, J. Garnaes, D.K. Schwartz, Science 263 (1994) 1726–1733.
[86] P. Bassereau, F. Pincet, Langmuir 13 (1997) 7003–7007.
[87] J. Mou, J. Yang, Z. Shao, J. Mol. Biol. 248 (1995) 507–512.
[88] S. Leporatti, F. Bringezu, G. Brezesinski, H. Möhwald, Langmuir 14 (1998) 7503–7510.
[89] H.A. Rinia, R.A. Demel, J.P.J.M. van der Eerden, B. de Kruijff, Biophys. J. 77 (1999) 1683–1693.
[90] Y. Fang, J. Yang, Biochim. Biophys. Acta 1324 (1997) 309–319.
[91] M.S. Malghani, J. Yang, J. Wu, J. Acoust. Soc. Am. 103 (1998) 1682–1685.
[92] I. Vikholm, J. Peltonen, O. Teleman, Biochim. Biophys. Acta 1233 (1995) 111–117.
[93] M. Beckmann, P. Nollert, H.-A. Kolb, J. Membr. Biol. 161 (1998) 227–233.
[94] S. Singh, D.J. Keller, Biophys. J. 60 (1991) 1401–1410.
[95] S.L. Brandow, D.C. Turner, B.R. Ratna, B.P. Gaber, Biophys. J. 64 (1993) 898–902.
[96] H.F. Knapp, W. Wiegräbe, M. Heim, R. Eschrich, R. Guckenberger, Biophys. J. 69 (1995) 708–715.
[97] T.M. Winger, E.L. Chaikof, Langmuir 14 (1998) 4148–4155.
[98] T.M. Winger, P.J. Ludovice, E.L. Chaikof, Langmuir 15 (1999) 3866–3874.
[99] T. Viitala, J. Peltonen, Biophys. J. 76 (1999) 2803–2813.
[100] Y. Chunbo, L. Xinmin, D. Desheng, L. Bin, Z. Hongjie, L. Zuhong, L. Juzheng, N. Jiazuan, Surf. Sci. 366 (1996) L729–L734.
[101] D.M. Czajkowsky, C. Huang, Z. Shao, Biochemistry 34 (1995) 12501–12505.
[102] Y. Fang, J. Yang, J. Phys. Chem. 100 (1996) 15614–15619.
[103] I. Reviakine, A. Simon, A. Brisson, Langmuir 16 (2000) 1473–1477.
[104] D.C. Turner, B.M. Peek, T.E. Wertz, D.D. Archibald, R.E. Geer, B.P. Gaber, Langmuir 12 (1996) 4411–4416.
[105] M. Grandbois, H. Clausen-Schaumann, H.E. Gaub, Biophys. J. 74 (1998) 2398–2404.
[106] L.K. Nielsen, J. Risbo, T.H. Callisen, T. Bjørnholm, Biochim. Biophys. Acta 1420 (1999) 266–271.
[107] N.C. Santos, E. Ter-Ovanesyan, J.A. Zasadzinski, M. Prieto, M.A.R.B. Castanho, Biophys. J. 75 (1998) 1869–1873.
[108] T.H. Ha, C.H. Kim, J.S. Park, K. Kim, Langmuir 16 (2000) 871–875.
[109] H. Egawa, K. Furusawa, Langmuir 15 (1999) 1660–1666.
[110] I. Reviakine, A. Brisson, Langmuir 16 (2000) 1806–1815.
[111] H.-A. Kolb, O. Enders, R. Schauer, Appl. Phys. A 68 (1999) 247–254.
[112] Z. Tang, W. Jing, E. Wang, Langmuir 16 (2000) 1696–1702.
[113] J.W. Carlson, A. Jonas, S.G. Sligar, Biophys. J. 73 (1997) 1184–1189.
[114] T. Shibata-Seki, J. Masai, T. Tagawa, T. Sorin, S. Kondo, Thin Solid Films 273 (1996) 297–303.
[115] B. Pignataro, C. Steinem, H.-J. Galla, H. Fuchs, A. Janshoff, Biophys. J. 78 (2000) 487–498.
[116] J.R. Abney, J. Braun, J.C. Owicki, Biophys. J. 52 (1987) 441–454.
[117] W. Curatolo, Biochim. Biophys. Acta 906 (1987) 111–136.
[118] M. Edidin, Curr. Top. Membr. Transp. 36 (1990) 81–96.
[119] P.K.J. Kinnunen, Chem. Phys. Lipids 57 (1991) 375–399.
[120] J.-F. Tocanne, L. Cézanne, A. Lopez, B. Piknova, V. Schram, J.-F. Tournier, M. Welby, Chem. Phys. Lipids 73 (1994) 139–158.
[121] X.M. Yang, D. Xiao, S.J. Xiao, Y. Wei, Appl. Phys. A 59 (1994) 139–143.
[122] X.M. Yang, D. Xiao, S.J. Xiao, Z.H. Lu, Y. Wei, Phys. Lett. A 193 (1994) 195–198.
[123] L. Santesson, T.M.H. Wong, M. Taborelli, P. Descouts, M. Liley, C. Duschl, H. Vogel, J. Phys. Chem. 99 (1995) 1038–1045.
[124] J. Masai, T. Shibata-Seki, K. Sasaki, H. Murayama, K. Sano, Thin Solid Films 273 (1996) 289–296.
[125] H. Shiku, R.C. Dunn, J. Phys. Chem. B 102 (1998) 3791–3797.
[126] C.W. Hollars, R.C. Dunn, J. Phys. Chem. B 101 (1997) 6313–6317.
[127] J. Hwang, L.K. Tamm, C. Böhm, T.S. Ramalingam, E. Betzig, M. Edidin, Science 270 (1995) 610–614.
[128] Y. Horiuchi, K. Yagi, T. Hosokawa, N. Yamamoto, H. Muramatsu, M. Fujihira, J. Microsc. 194 (1999) 467–471.
[129] H. Shiku, R.C. Dunn, J. Microsc. 194 (1999) 455–460.
[130] H. Shiku, R.C. Dunn, J. Microsc. 194 (1999) 461–466.

[131] E. ten Grotenhuis, R.A. Demel, M. Ponec, D.R. Boer, J.C. van Miltenburg, J.A. Bouwstra, Biophys. J. 71 (1996) 1389–1399.
[132] J.M. Solletti, M. Botreau, F. Sommer, T. Minh Duc, M.R. Celio, J. Vac. Sci. Technol. B 14 (1996) 1492–1497.
[133] Y.F. Dufrêne, W.R. Barger, J.-B.D. Green, G.U Lee, Langmuir 13 (1997) 4779–4784.
[134] C. DeWolf, S. Leporatti, C. Kirsch, R. Klinger, G. Brezesinski, Chem. Phys. Lipids 97 (1999) 129–138.
[135] A.L. Weisenhorn, F.-J. Schmitt, W. Knoll, P.K. Hansma, Ultramicroscopy 42–44 (1992) 1125–1132.
[136] C. Gliss, H. Clausen-Schaumann, R. Günther, S. Odenbach, O. Randl, T.M. Bayerl, Biophys. J. 74 (1998) 2443–2450.
[137] G. Valdrè, A. Alessandrini, U. Muscatello, U. Valdrè, V. Vannini, Philos. Mag. B 79 (1999) 1549–1559.
[138] C.W. Hollars, R.C. Dunn, Biophys. J. 75 (1998) 342–353.
[139] D.M. Czajkowsky, M.J. Allen, V. Elings, Z. Shao, Ultramicroscopy 74 (1998) 1–5.
[140] V. Vié, N. Van Mau, E. Lesniewska, J.P. Goudonnet, F. Heitz, C. Le Grimellec, Langmuir 14 (1998) 4574–4583.
[141] X.M. Ping, S.J. Xiao, Z.H. Lu, Y. Wei, Surf. Sci. 316 (1994) L1110–L1114.
[142] X.M. Yang, S.J. Xiao, Z.H. Lu, Y. Wei, Surf. Sci. 316 (1994) L1110–L1114.
[143] I. Vikholm, J. Peltonen, Thin Solid Films 284–285 (1996) 924–926.
[144] Y. Dori, H. Bianco-Peled, S.K. Satija, G.B. Fields, J.B. McCarthy, M. Tirrell, J. Biomed. Mater. Res. 50 (2000) 75–81.
[145] J. Mou, D.M. Czajkowsky, Z. Shao, Biochemistry 35 (1996) 3222–3226.
[146] N. Van Mau, V. Vié, L. Chaloin, E. Lesniewska, F. Heitz, C. Le Grimellec, J. Membr. Biol. 167 (1999) 241–249.
[147] V. Vié, N. Van Mau, L. Chaloin, E. Lesniewska, C. Le Grimellec, F. Heitz, Biophys. J. 78 (2000) 846–856.
[148] T.L. Fare, C.A. Palmer, C.G. Silvestre, D.H. Cribbs, D.C. Turner, S.L. Brandow, B.P. Gaber, Langmuir 8 (1992) 3116–3121.
[149] M. Amrein, A. vonNahmen, M. Sieber, Eur. Biophys. J. 26 (1997) 349–357.
[150] A. von Nahmen, M. Schenk, M. Sieber, M. Amrein, Biophys. J. 72 (1997) 463–469.
[151] I. Panaiotov, Tz. Ivanova, J. Proust, F. Boury, B. Denizot, K. Keough, S. Taneva, Colloid Surf. B Biointerface 6 (1996) 243–260.
[152] R. Grunder, P. Gehr, H. Bachofen, S. Schürch, H. Siegenthaler, Eur. Respir. J. 14 (1999) 1290–1296.
[153] P. Kernen, W.I. Gruszecki, M. Matula, P. Wagner, U. Ziegler, Z. Krupa, Biochim. Biophys. Acta 1373 (1998) 289–298.
[154] H. Lin, Y.J. Zhu, R. Lal, Biochemistry 38 (1999) 11189–11196.
[155] K. Ekelund, L. Eriksson, E. Sparr, Biochim. Biophys. Acta 1464 (2000) 1–6.
[156] D.J. Müller, A. Engel, M. Amrein, Biosens. Bioelectron. 12 (1997) 867–877.
[157] Y. Fang, J. Yang, J. Phys. Chem. B 101 (1997) 441–449.
[158] M.S. Malghani, J. Yang, J. Phys. Chem. B 102 (1998) 8930–8933.
[159] I.T. Dorn, U.G. Hofmann, J. Peltonen, R. Tampé, Langmuir 14 (1998) 4836–4842.
[160] H. Clausen-Schaumann, H.E. Gaub, Langmuir 15 (1999) 8246–8251.
[161] S. Kasas, F. Hofmann, M.R. Celio, E. Carafoli, Scanning 14 (1992) 276–281.
[162] K. Takeyasu, H. Omote, S. Nettikadan, F. Tokumasu, A. Iwamoto-Kihara, M. Futai, FEBS Lett. 392 (1996) 110–113.
[163] S. Singh, P. Turina, C.J. Bustamante, D.J. Keller, R. Capaldi, FEBS Lett. 397 (1996) 30–34.
[164] D. Neff-D, S. Tripathi, K. Middendorf, H. Stahlberg, H.-J. Butt, E. Bamberg, N.A. Dencher, J. Struct. Biol. 119 (1997) 139–148.
[165] J.D. Burgess, V.W. Jones, M.D. Porter, M.C. Rhoten, F.M. Hawkridge, Langmuir 14 (1998) 6628–6631.
[166] S. Boussaad, L. Dziri, R. Arechabaleta, N.J. Tao, R.M. Leblanc, Langmuir 14 (1998) 6215–6219.
[167] O.I. Kiselyova, O.L. Guryev, A.V. Krivosheev, S.A. Usanov, I.V. Yaminsky, Langmuir 15 (1999) 1353–1359.
[168] T.H. Bayburt, J.W. Carlson, S.G. Sligar, J. Struct. Biol. 123 (1998) 37–44.
[169] I.T. Dorn, R. Eschrich, E. Seemüller, R. Guckenberger, R. Tampé, J. Mol. Biol. 288 (1999) 1027–1036.
[170] T.J. Beveridge, Curr. Opin. Struct. Biol. 4 (1994) 204–212.
[171] U.B. Sleytr, T.J. Beveridge, Trends Microbiol. 7 (1999) 253–260.
[172] B. Wetzer, D. Pum, U.B. Sleytr, J. Struct. Biol. 119 (1997) 123–128.
[173] F.-J. Schmitt, A.L. Weisenhorn, P.K. Hansma, W. Knoll, Thin Solid Films 210/211 (1992) 666–669.
[174] S. Scheuring, D.J. Müller, P. Ringler, J.B. Heymann, A. Engel, J. Microsc. 193 (1999) 28–35.
[175] I. Reviakine, W. Bergsma-Schutter, A. Brisson, J. Struct. Biol. 121 (1998) 356–361.
[176] D.M. Czajkowsky, H. Iwamoto, T.L. Cover, Z. Shao, Proc. Natl. Acad. Sci. USA 96 (1999) 2001–2006.
[177] H. Iwamoto, D.M. Czajkowsky, T.L. Cover, G. Szabo, Z. Shao, FEBS Lett. 450 (1999) 101–104.
[178] Y. Fang, S. Cheley, H. Bayley, J. Yang, Biochemistry 36 (1997) 9518–9522.
[179] D.M. Czajkowsky, S. Sheng, Z. Shao, J. Mol. Biol. 276 (1998) 325–330.
[180] M.S. Malghani, Y.E. Fang, S. Cheley, H. Bayley, J. Yang, Microsc. Res. Tech. 44 (1999) 353–356.
[181] G. Zuber, E. Barklis, Biophys. J. 78 (2000) 373–384.
[182] F.A. Schabert, C. Henn, A. Engel, Science 268 (1995) 92–94.
[183] D.J. Müller, A. Engel, J. Mol. Biol. 285 (1999) 1347–1351.
[184] T. Walz, P. Tittmann, K.H. Fuchs, D.J. Müller, B.L.

Smith, P. Agre, H. Gross, A. Engel, J. Mol. Biol. 264 (1996) 907–918.
[185] S. Scheuring, P. Ringler, M. Borgnia, H. Stahlberg, D.J. Müller, P. Agre, A. Engel, EMBO J. 18 (1999) 4981–4987.
[186] H.-J. Butt, M. Jaschke, W. Ducker, Bioelectrochem. Bioenerg. 38 (1995) 191–201.
[187] N.A. Burnham, R.J. Colton, in: D.A. Bonnell (Ed.), Scanning Tunneling Microscopy and Spectroscopy: Theory, Technique and Applications, VCH, New York, 1996, pp. 191–249.
[188] R.W. Carpick, M. Salmeron, Chem. Rev. 97 (1997) 1163–1194.
[189] B. Cappella, G. Dietler, Surf. Sci. Rep. 34 (1999) 1–104.
[190] T.J. Senden, C.J. Drummond, P. Kékicheff, Langmuir 10 (1994) 358–362.
[191] S.J. O'Shea, M.E. Welland, T. Rayment, Appl. Phys. Lett. 60 (1992) 2356–2358.
[192] S.J. O'Shea, M.E. Welland, T. Rayment, Appl. Phys. Lett. 61 (1992) 2240–2242.
[193] J.P. Cleveland, T.E. Schäffer, P.K. Hansma, Phys. Rev. B 52 (1995) R8692–R8695.
[194] N.A. Burnham, D.D. Dominguez, R.L. Mowrey, R.J. Colton, Phys. Rev. Lett. 64 (1990) 1931–1934.
[195] A.L. Weisenhorn, M. Khorsandi, S. Kasas, V. Gotzos, H.-J. Butt, Nanotechnology 4 (1993) 106–113.
[196] E.W. van der Vegte, G. Hadziioannou, Langmuir 13 (1997) 4357–4368.
[197] S.P. Jarvis, A. Oral, T.P. Weihs, J.B. Pethica, Rev. Sci. Instrum. 64 (1993) 3515–3520.
[198] S.P. Jarvis, H. Yamada, S.-I. Yamamoto, H. Tokumoto, J.B. Pethica, Nature 384 (1996) 247–249.
[199] S.J. O'Shea, M.E. Welland, J.B. Pethica, Chem. Phys. Lett. 223 (1994) 336–340.
[200] M.A. Lantz, S.P. Jarvis, H. Tokumoto, T. Martynski, T. Kusumi, C. Nakamura, J. Miyake, Chem. Phys. Lett. 315 (1999) 61–68.
[201] Y. Martin, C.C. Williams, H.K. Wickramasinghe, J. Appl. Phys. 61 (1987) 4723–4729.
[202] J.P. Cleveland, B. Anczykowski, A.E. Schmid, V.B. Elings, Appl. Phys. Lett. 72 (1998) 2613–2615.
[203] S.N. Magonov, in: R.A. Meyers (Ed.), AFM in Analysis of Polymers, Encyclopedia of Analytical Chemistry, Wiley-VCH, Chichester, UK, in press.
[204] L. Wang, Appl. Phys. Lett. 73 (1998) 3781–3783.
[205] S.J.T. van Noort, O.H. Willemsen, K.O. van der Werf, B.G. de Grooth, J. Greve, Langmuir 15 (1999) 7101–7107.
[206] T.R. Albretch, C.F. Quate, J. Vac. Sci. Technol. A. 6 (1988) 271–274.
[207] S.S. Shieko, M. Moller, E.M.C.M. Reuvekamp, H.W. Zandbergen, Phys. Rev. B 48 (1993) 5675–5678.
[208] G.U Lee, L.A. Chrisey, C.E. O'Ferrall, D.E. Pilloff, N.H. Turner, R.J. Colton, Israel J. Chem. 36 (1996) 81–87.
[209] Y.S. Lo, N.D. Huefner, W.S. Chan, P. Dryden, B. Hagenhoff, T.P. Beebe, Langmuir 15 (1999) 6522–6526.
[210] Y.I. Rabinovich, R.H. Yoon, Langmuir 10 (1994) 1903–1909.
[211] H. Dai, J.H. Hafner, A.G. Rinzler, D.T. Colbert, R.E. Smalley, Nature 384 (1996) 147–150.
[212] S.S. Wong, E. Joselevich, A.T. Woolley, C.L. Cheung, C.M. Lieber, Nature 394 (1998) 52–55.
[213] B. Derjaguin, Kolloid Z. 69 (1934) 155–164.
[214] J. Schneider, Y.F. Dufrêne, W.R. Barger, G.U Lee, Biophys. J. 79 (2000) 1107–1118.
[215] H.-J. Butt, Biophys. J. 60 (1991) 777–785.
[216] R. Raiteri, M. Grattaraola, H.-J. Butt, J. Phys. Chem. 100 (1996) 16700–16705.
[217] C.J. Drummond, T.J. Senden, Colloid Surf. A: Physicochem. Eng. Asp. 87 (1994) 217–234.
[218] T.J. Senden, C.J. Drummond, Colloid Surf. A: Physicochem. Eng. Asp. 94 (1995) 29–51.
[219] K.L. Johnson, Contact Mechanics, Cambridge University Press, Cambridge, 1985.
[220] D.D. Koleske, W.R. Barger, G.U Lee, R.J. Colton, Mater. Res. Soc. Symp. Proc. 464 (1997) 377–383.
[221] J. Schneider, W. Barger, G. Lee, Biophys. J. (2000) submitted for publication.
[222] D.M. Le Neveu, R.P. Rand, V.A. Parsegian, Nature 259 (1976) 601–603.
[223] J. Marra, J. Israelachvili, Biochemistry 24 (1985) 4608–4618.
[224] E.A. Evans, Biophys. J. 31 (1980) 425–432.
[225] C.E.H. Berger, K.O. van der Werf, R.P.H. Kooyman, B.G. de Grooth, J. Greeve, Langmuir 11 (1995) 4188–4192.
[226] W.A. Ducker, D.R. Clarke, Colloid Surf. A: Physicochem. Eng. Asp. 94 (1994) 275–292.
[227] C. Rotsch, M. Radmacher, Langmuir 13 (1997) 2825–2832.
[228] A.T.A. Jenkins, N. Boden, R.J. Bushby, S.D. Evans, P.F. Knowles, R.E. Miles, S.D. Ogier, H. Schönherr, G.J. Vancso, J. Am. Chem. Soc. 121 (1999) 5274–5280.
[229] S. Xu, M.F. Arnsdorf, Proc. Natl. Acad. Sci. USA 92 (1995) 10384–10388.
[230] R. Ishiguro, D.Y. Sasaki, C. Pacheco, K. Kurihara, Colloid Surf. A: Physicochem. Eng. Asp. 146 (1999) 329–331.
[231] W.F. Heinz, J.H. Hoh, Biophys. J. 76 (1999) 528–538.
[232] W. Xu, B.L. Blackford, J.G. Cordes, M.H. Jericho, D.A. Pink, V.G. Levadny, T. Beveridge, Biophys. J. 72 (1997) 1404–1413.
[233] H.-J. Butt, Biophys. J. 63 (1992) 578–582.
[234] D.J. Müller, D. Fotiadis, S. Scheuring, S.A. Müller, A. Engel, Biophys. J. 76 (1999) 1101–1111.
[235] Y.F. Dufrêne, Micron 32 (2001) 153–165.
[236] H. Mueller, H.-J. Butt, E. Bamberg, Biophys. J. 76 (1999) 1072–1079.
[237] A. Engel, H.E. Gaub, D.J. Müller, Curr. Biol. 9 (1999) R133–R136.